SYNTHESIS, CHARACTERIZATION, PHYSICOCHEMICAL PROPERTIES AND SENSING APPLICATION OF LANTHANIDE-BASED METAL ORGANIC FRAMEWORKS

Sandhya Singh

A dissertation submitted for the partial fulfillment of B.S.-M.S. Dual Degree in Science

Indian Institute of Science Education and Research Mohali

April 2016

Certificate of Examination

This is to certify that the dissertation titled "Synthesis, Characterization, Physicochemical Properties and Sensing Application of Lanthanide-based Metal Organic Frameworks" submitted by Ms. Sandhya Singh (Reg. No. MS11038) for the partial fulfillment of BS-MS dual degree programme of the Institute has been examined by the thesis committee members duly appointed by the Institute. The committee finds the work done by the candidate satisfactory and recommends that the thesis be accepted.

Dr. Ramesh Ramachandran	Dr. Sugumar Venkataramani	Prof. Sanjay Mandal
(Member)	(Member)	(Convener & Supervisor)

Dated: April 22, 2016

Declaration

The work presented in this dissertation has been carried out by me under the guidance of Prof. Sanjay Mandal at the Indian Institute of Science Education and Research Mohali. This work has not been submitted in part or in full for a degree, a diploma, or a fellowship to any other university or institute. Whenever contributions of others are involved, every effort is made to indicate this clearly, with due acknowledgement of collaborative research and discussions. This thesis is a bonafide record of original work done by me and all sources listed within have been detailed in the bibliography.

Sandhya Singh

Dated: April 22, 2016

In my capacity as the supervisor of the candidate's project work, I certify that the above statements by the candidate are true to the best of my knowledge.

Prof. Sanjay Mandal

Dated: April 22, 2016

Acknowledgements

I would like to express my gratitude to my supervisor Professor Sanjay K. Mandal for his guidance, interesting ideas on the project and encouragement throughout my research work. I appreciate his precious time and valuable advice for my research and revising my thesis.

I would also like to sincerely thank Dr. Sadhika Khullar as the thesis co-director whose help and support during this work were essential to me.

I also thank my committee members Dr. Ramesh Ramachandran and Dr. Sugumar Venkataramani. I appreciate the contributions of Sandeep Kumar, Datta Markad and Prasenjit Das for their invaluable help and support and willingness to always assist me in conducting my experiments. I also thank other members of the Mandal group - Navnita Kumar, Biswajit Laha, Vijay Gupta, Gouri Chakrabourty, Shardha Gandhi, Smriti Thakur, Alisha Gogia, and Sheeba Khan.

I would like to thank all faculty members whose courses I have taken during my BS-MS studies. I gratefully acknowledge the infrastructure and support in the Department of Chemical Sciences, Indian Institute of Science Education and Research Mohali.

Last but not least, I am eternally grateful to God, my family and friends for their endless love and support throughout my studies.

List of Figures

List of Schemes

List of Tables

Contents

Abstract

In the last few decades, Lanthanide coordination compounds have been of intense interest for their practical applications in sensing, radioactive labelling, time resolved fluoroimmunoassays, bio-imaging, etc. Modulation of their characteristic luminescence is the key to these applications. Lanthanide ions are sensitized via an "antenna effect" through the coordination of N/O donor ligands acting as chromophores to obtain highly intense luminescence from the Lanthanide centre, which normally show Laporte forbidden *f-f* transitions with low intensity emission bands. In this work, a pyridine-carboxylate based ligand such as potassium 2,2'-(butane-1,4-diylbis((pyridin-2-ylmethyl)azanediyl))diacetate (K_2bpbd), which is prepared in high yield and spectroscopically characterized, has been utilized to make nine new lanthanide complexes namely, $\{[Ln(bpbd)(H_2O)_2(X)]\cdot y(H_2O)\}_n$, where Ln = La (**1**, **6** and **7**), Nd (**2**, **8** and **9**), Sm (**3**), Tb (**4**) and Dy (**5**); X^- = NO_3^- (**1**, **2**, **3**, **4** and **5**), OAc^- (**6** and **8**), Cl^- (**7**) and ClO_4^- (**9**); y = 7 for **1**, **2**, **3** and **8** and = 5 for **4**-**7**. All these Ln-MOFs were extensively characterized by various spectroscopic techniques (UV-vis and FTIR), elemental analyses, thermogravimetric analysis and powder X-ray diffractometry. All but La complexes show very intense characteristic luminescence features that confirm the antenna effect of the ligand on the metal centre. Complexes **2**, **4**, **8** and **9** display selective sensing of trinitrophenol (TNP) in water with the best detection limit of 1 ppm for **4**.

Chapter I

Introduction

1.1 Porous Materials

Until mid 1990, there were two types of porous materials, *e.g.*, inorganic (zeolites, for example) and organic (activated carbon, for example) materials (Figure 1). Porous solids are classified into three categories based on their pore size: microporous (2 nm or smaller), mesoporous (2-50 nm) and macroporous (> 50 nm).[1-3] Zeolites, naturally occurring minerals, are one of the examples of microporous materials.[4] Zeolites are purely inorganic materials, made by 3D framework of aluminosilicates/aluminophosphates. Zeolities have various applications in industry for catalysis, xylene isomerisation, detergents and water softners.[4] Activated carbons are purely organic polymers with high porosity and high surface area.

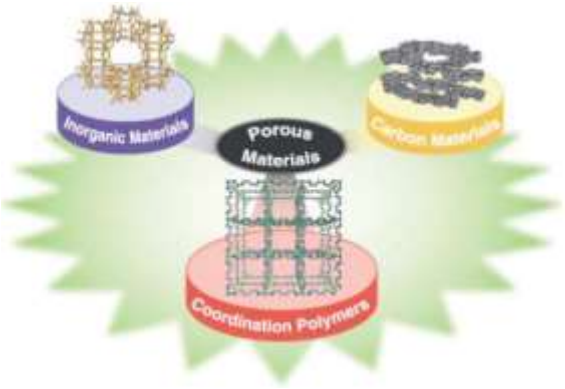

Figure 1. Classes of Porous Materials (adapted from reference 5).

1.2 Overview of Metal Organic Frameworks

The coordination polymers are infinite arrays of metal ions and bridging ligand which can grow in different directions to form 1D, 2D and 3D networks.[6] The backbone of a coordination polymer is constructed from the self assembly and simple combination of the metal nodes as connectors and multitopic bridging ligands, where the bridging ligands can be inorganic (like N_3^-, CN^-, CNO^-, etc), metallo-ligand (for example, $[Ag/Au(CN)_2]^-$) or organic like picolinate, different aromatic or aliphatic polycarboxylate, etc. When the network is solely built by metal ions/metal clusters and bridged by organic linkers, they are termed as metal organic frameworks (MOFs). For the past 20 years, the emergence of MOFs as new porous materials has kept many fields in science busy in exploring their applications in numerous areas.

The construction of the desired architectural, physical and chemical properties of MOFs depends on the properties of the linker and the connecting metals.[7] In general, a linker can be anionic or neutral. In most cases, a neutral ligand serves as pillars and further increases the dimensionality. The basic features of the MOFs materials are governed by the number of binding sites on the metal centre and their relative orientation, Lewis basic sites on a ligand and their mode of coordination, and the relative angularity of these sites (Figure 2).

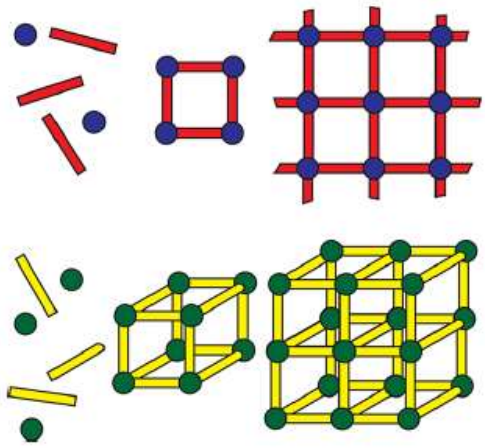

Figure 2. Self-assembly *via* connectors and linear linkers (adapted from reference 8).

1.3 Straightforward Synthetic Methods

MOFs can be synthesized via different synthetic strategies like hydrothermal/solvothermal synthesis, one pot, simple diffusion method, microwave assisted synthesis, mechanochemical synthesis, etc.

Hydrothermal/*Solvothermal Synthesis*: Hydrothermal synthesis is one of the techniques of crystallization, where the starting materials are allowed to react at high temperature and at an autogenous pressure. Most of the reported MOFs have been synthesized using hydrothermal/solvothermal synthetic conditions, often by using Teflon lined sealed autoclaves. In case of hydrothermal synthesis, water is used as a solvent whereas in solvothermal synthesis various organic solvents are used. Other than this, a mixtures of water and organic solvents also have been used to prepare various MOFs. Small changes in one or more of the reaction conditions, such as temperature, time, pH or the solvent type can have an influence on the formation of the product.

Diffusion technique: In this synthetic technique, a solution containing the metal salt or metal cluster diffuses into another solution containing organic ligand(s). This is a slow technique and generally gives low yield.[9]

Mechanochemical Approach: Their synthesis can also be possible from using mechanochemistry, that is, grinding of two or more solids through a mechanical ball mill and thereby avoiding the use of solvents.[9] Klimakow *et al*. have reported the synthesis of HKUST-1 ($Cu_3(BTC)_2$, BTC= 1,3,5-benzenetricarboxylate) and MOF14 ($Cu_3(BTB)_2$, BTB= 4,4',4''-benzenetribenzoate) by this method.[9]

1.4 Applications of MOFs

Gas storage/separation: MOFs have high surface area, crystallinity and tunable properties. Because of these properties, MOFs have attracted intense interest for gas capture and storage. The adsorption of gas molecules on the surface of MOFs plays a crucial role in correlating structural features of the compound. The adsorption phenomenon not only gives information about the interaction of adsorbent and adsorbate but also indicates the pore size and shape.

Catalysis: MOFs can be used as catalysts through i) coordinatively unsaturated metal centre, ii) metal complexes (as homogeneous catalyst) and iii) ligand-functionalised with organic group(s). Long *et al*. reported the synthesis of microporous $Mn_3[(Mn_4Cl)_3BTT_8(CH_3OH)_{10}]_2$ (H_3BTT = 1,3,5-benzenetristetrazol-5-yl) that selectively catalyze the transformation of aldehydes and ketones to the corresponding cyanosilylated products in the presence of cyanotrimethylsilane in good yields.[10]

Sensing: There are several ways to make luminescent MOFs (Figure 3).[11] The best way to make luminescent MOFs is to incorporate luminescent inorganic or organic ligand moiety in the framework. The most common choice is the incorporation of the lanthanide ions, example Eu(III) and Tb(III) which give red and green luminescence, respectively. There are several ways to use luminescent MOFs as efficient sensors. One of the examples is shift in the wavelength due to external stimuli. Lee *et al*. have reported the shift in wavelength of the $[Zn_4O(NTB)_2]$ (where H_3NTB = 4,4',4''-nitrilotrisbenzoic acid) depending on the presence of guest molecule such as DMF or EtOH.[12] Thus the presence of solvents can be detected by using such MOFs.

Another detection mode is the change in luminescence intensity. Based on the external stimuli, which can be any solvent, anionic/cationic or neutral compound, the luminescence intensity get

enhanced or quenched. For example, a Europium based MOF, Eu(BTC), revealed significant increase in the intensity when it gets exposed to DMF and showed observable quenching after exposure of acetone.[14] Xiao *et al*. reported the selective detection of the picric acid over the other nitroaromatics with a detection limit of 8.1 x 10^{-8} M.[13]

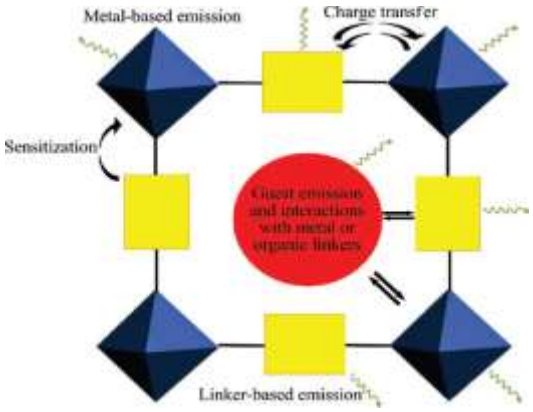

Figure 3. Emission possibilities in a porous MOF (adapted from reference 11).

1.5 Lanthanide based Metal Organic Frameworks (Ln-MOFs)

In recent years Ln-MOFs have been of great interests due to their photoluminescence and magnetic properties.[14, 15] However, their application as porous materials in gas/solvent adsorption have been less explored.[16] The different kinds of organic linkers or ligands used for the construction of Ln-MOFs are mostly carboxylate based, which attracted more attention due to its potential to give porous structures. Rosi *et al*. synthesized a series of metal cluster of rod shaped Ln-MOFs by using 1,3,5-benzenetricarboxylates (BTC).[17] Luo *et al*. also used BTC to synthesize the porous [$Y(BTC)(H_2O)\cdot 4.3H_2O$] (Y-MOF) which possesses tetragonal pores with approximately 6Å pore size and shows selective sorption for hydrogen over nitrogen gas.[18] The capacity of Y-MOF for hydrogen uptake is 28.8 g/L at 77 K and 10 bar pressure.

Thus, porosity of MOFs plays a significant role in the several applications such as, gas/solvent sorption, drug delivery, catalysis, sensing etc. porosity can be increased via extending the ligand or linker length; however, sometimes it may cause interpenetration of the frameworks. Several groups (Rosi *et al.*, Ma *et al.* and Zhang *et al*.) have reported different strategies to control the interpenetration. He *et al*. reported the first example of controlling interpenetration in Ln-MOFs.[19] They have reported a series of porous Ln-MOFs; [$Er_2(BDC)_3(phen)_2\cdot 3H_2O$,

$Tm_2(TBDC)_3(DMF)_2(H_2O)_2{\cdot}4H_2O$, $Er_2(TBDC)_3(phen)_2{\cdot}4DMF{\cdot}2H_2O$], where sterically bulky ligand and terminal chelating ligand are used to replace 1,4-benzenedicarboxylate (BDC) and coordinated solvent molecules.

Lanthanide complexes are very important in the field of analytical biology, radioactive labels[20] , diagnosis[21], contrast agents for nuclear magnetic resonance imaging[22], magnetic probes[23], luminescence microscopy[24] and time resolved fluoroimmunoassays.[25] These are also used for the construction of lamp phosphors,[26] organic light emitting diodes (OLED),[27, 28] optical fibers for telecommunications.[26] Those ions which emit in the near infrared region have found applications in lasers and are also interesting for telecommunications and optical amplifiers.[28, 30]

2.1 General Introduction to Lanthanides

In the periodic table, Lanthanides are situated at the bottom of the periodic table. It is comprised of group 15 elements ranging from Lanthanum (Z = 57) to Lutetium (Z = 71) (Figure 4). These are known as *f*-block elements where the gradual filling of the last electron in 4*f* orbital of the antepenultimate shell. The outer electronic configuration is generally $[Xe]4f^{n+1}6s^2$.

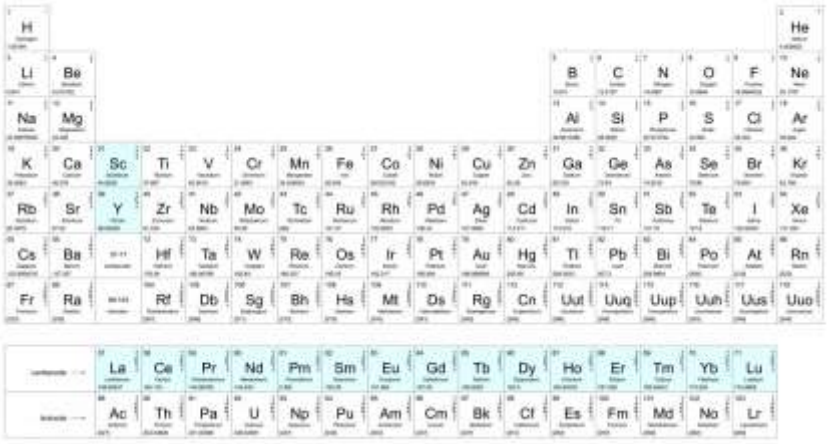

Figure 4. Periodic table showing lanthanides with a blue color (adapted from reference 31).

Atomic radius of lanthanide series decreases from left to right (Z= 58 to Z= 71) because of an increase in effective nuclear charge and poor shielding of the 4*f* orbitals. This phenomenon is known as lanthanide contraction. As a consequence of larger ionic radius of Ln(III) ions, these possess labile coordination sphere and weak stereochemical preference which leads to a high coordination number (3 to 12) and uncontrollable geometry. [32]

Usually, the stable oxidation state observed for lanthanide elements is +3, removing one electron from 4*f* and two electrons from 6*s* orbital; however, the exceptions are Ce^{4+}, Eu^{2+}, Sm^{2+}, Yb^{2+} and Tb^{4+} due to empty, half filled or fully filled 4*f* shell. The 4*f* orbitals are well shielded by the xenon core, which transforms the valence 4*f* orbitals into "inner orbitals". This phenomenon is the key to the chemical and spectroscopic properties of the lanthanide ions. An important characteristic feature of the lanthanide ions is photoluminescence. Several lanthanide ions show luminescence in the visible or near-infrared spectral regions upon irradiation with ultraviolet or visible radiation. This is discussed further below.

2.2 Structural Features of Lanthanides

Lanthanide based metal organic frameworks show fascinating structural properties because of their larger coordination sphere which is due to lack of any directional bonding character and large ionic size resulting into more flexible coordination geometry leading to the formation of uncontrollable topology. Ln(III) ions are hard Lewis acids and have high charge density and thus these prefer to bind with hard Lewis base *viz*, oxygen and form electrostatic bond. Since 4*f* electrons are buried inside, the mixing of ligand and metal orbitals are insignificant, consequently the bond between Ln(III) and ligand is non-directional. Generally, Ln(III) complexes show high coordination number (>6) but most commonly 8-9 due to lack of directional bonding. The most common geometry for lanthanide complexes in solid state are square antiprismatic, dodecahedral (for CN = 8), monocapped square anti prismatic and tricapped trigonal prismatic (for CN = 9), bicapped dodecahedral and bicapped square antiprismatic (for CN = 10), as shown in Figure 5.[32]

The structure of lanthanide based MOF can be controlled by metal ligand interaction, interligand steric constraints. A high ionic character of lanthanides mean these can favour to bind with the atoms which are hard Lewis bases, and hence combination of carboxylate and amine are ordinarily used in lanthanide complexation because amine groups are easily polarised.[32]

2.3 Spectral Features of Lanthanides

2.3.1 Electronic levels

Energy levels and the splitting pattern of ground and excited states of lanthanide ions can be described by the Russell-Saunders coupling scheme.[34] These energy levels of lanthanide ions can

be calculated considering the interactions between the 4*f* electrons. The 4*f* electrons give rise to a large number of excited states, shown in Figure 6, whose relative energies are determined by the combination of inter-electronic repulsions, spin-orbit coupling and ligand field effects; for example, Eu(III) $4f^6$ and Tb(III) $4f^8$ configurations give large number of states.[35]

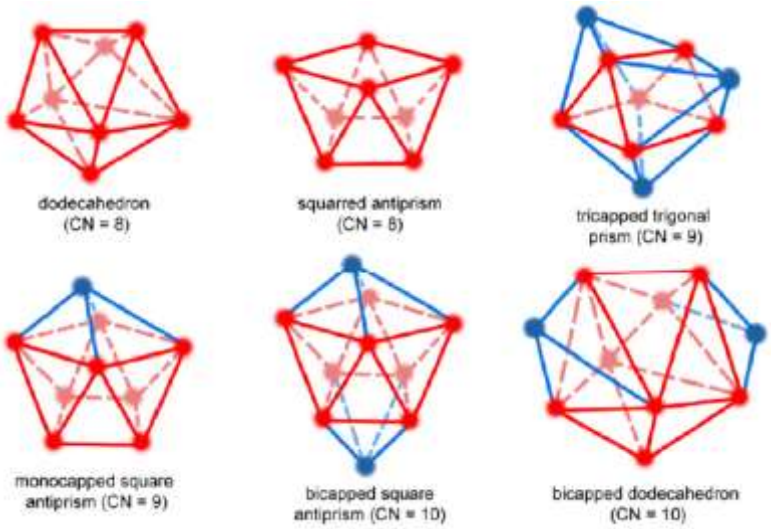

Figure 5. Usual coordination geometry around lanthanide ions.

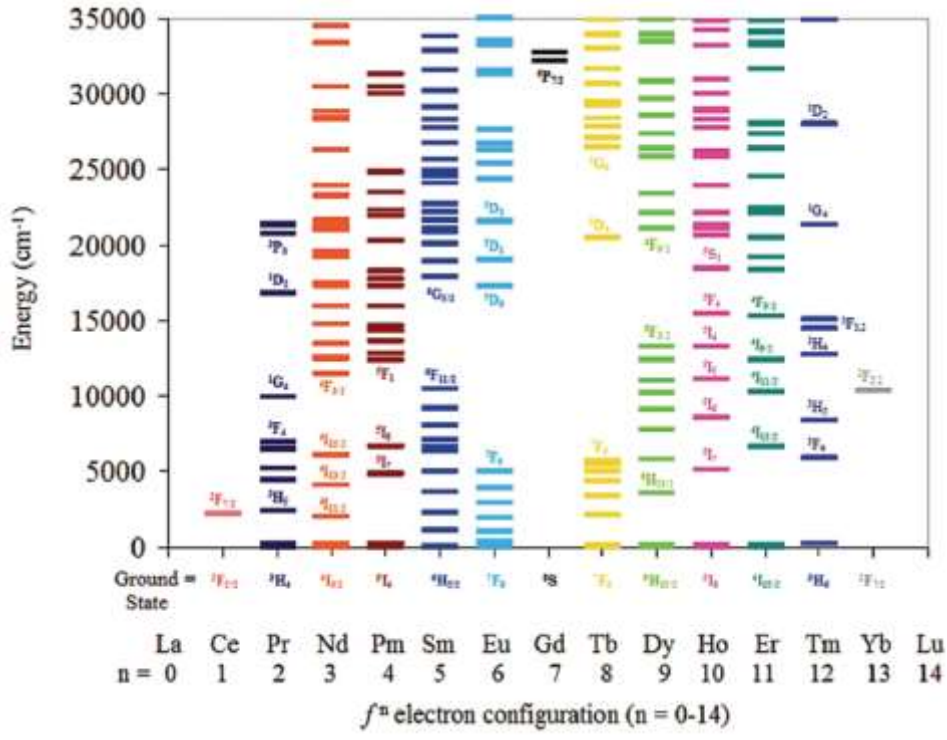

Figure 6. Energy level diagram for lanthanide ions (adapted from reference 33).

2.3.2 Electronic transitions

As a consequence of their relatively small radial extension, the 4*f* orbitals are effectively shielded from the environment by the filled 5*s* and 5*p* sub-shells and are only minimally involved in bonding. This has two important effects on the lanthanide emission and absorption spectroscopy. First, the ligand field splitting is very small, typically between 100 and 250 cm^{-1}. When an *f-f* electronic transition occurs, the spectral bands are very sharp and are similar to the emission bands observed for the free ions. Unlike the organic molecule or *d*-block complexes, the emission bands of lanthanide complexes are very sharp, narrow and show a very small Stoke's shift because the promotion of electrons into the higher energy 4*f* orbitals doesn't significantly disturb the geometry of the excited state (Figure 7).[36]

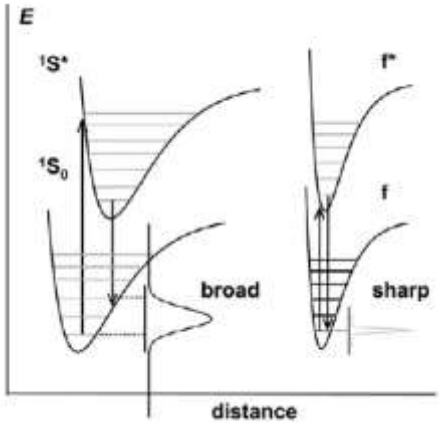

Figure 7. Configurational coordinate diagram: i) organic chromophore (left) ii) and lanthanide ion (right) (adapted from reference 36).

The electronic transitions follow the selection rule:

$$\langle v_f | \mu | v_i \rangle$$

Where ν_f and ν_i are the final and initial electronic state of transition, respectively, and μ is the operator which can be electronic dipole, magnetic dipole, etc.

Electronic dipole transitions are forbidden by the parity (Laporte) selection rule, which does not allow transitions among orbitals having the same symmetry.[37] Nonetheless, when the lanthanide ion is under the influence of a ligand field, non-centrosymmetric interactions somewhat relax the selection rules. Hypothetically, magnetic dipole transitions are allowed by the parity rule and are weak and their intensity is rather insensitive to the Ln(III) environment. Another type of

transitions also possible in lanthanide ions are i) 4*f*-5*d* transition and ii) the charge transfer transitions.[37]

i) 4*f*-5*d* transitions: 4*f*-5*d* transitions are parity allowed where 4*f* electron promotes into 5*d* orbital. Therefore, these transitions are broader and have high intensity than *f-f* transitions because 5*d* orbital directly interacts with ligand orbitals and only observed in Ce(III), Pr(III) and Tb(III).

ii) Charge transfer transitions: These are generally two types i) metal to ligand charge transfer (MLCT) ii) ligand to metal charge transfer (LMCT). Both MLCT and LMCT are parity allowed transitions. These transitions have very high energies, appearing in the UV region of electromagnetic spectrum.

2.3.3 Luminescence

Luminescence is a phenomenon shown by the materials which absorb the radiation in certain region and emit spontaneously in the form of light.[38] The term "luminescence" was coined by a German physicist Eilhardt Wiedemann in 1888.[39] The Jablonski diagram (Figure 8) explains the mechanism of luminescence.[40] It is subdivided into two categories of non-radiative emission transitions:- i) fluorescence and ii) phosphorescence. Fluorescence is the light emission phenomenon resulting from the S_1 (singlet excited state) $\rightarrow$ S_0 (singlet ground state) transition and ends in 10^{-9}-10^{-7} s.[40] Phosphorescence is the light emission resulting from the T_1 (triplet excited state) $\rightarrow$ S_0 (singlet ground state) transition; the transition occurs between energy states with different spin multiplicities.[40] Since phosphorescence is a spin-forbidden transition, the

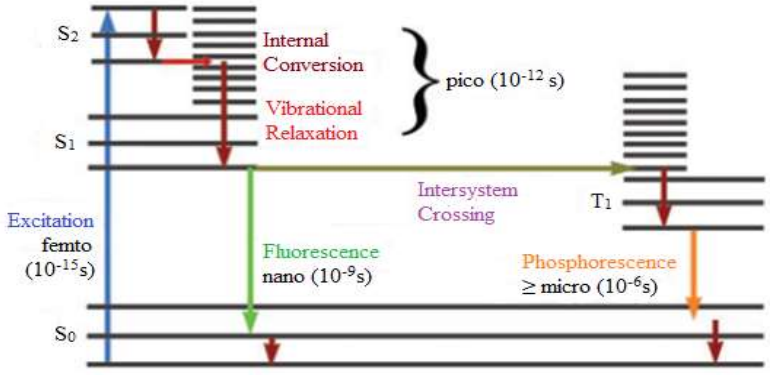

Figure 8. Jablonski diagram (adapted from reference 40).

emission lifetime is longer (10^{-3}-10^{0} s) than fluorescence.[40] The singlet excited states can become triplet excited states through intersystem crossing. There are also different forms of luminescence based on the source of excitation (Table 1).[38] Mainly photoluminescence will be discussed in this thesis.

Table 1. Different forms of luminescence.

Type of luminescence	*Excitation source*
Electroluminescence	Electric field
Photoluminescence	Light absorption
Chemiluminescence	Chemical process
Radioluminescence	Ionizing radiation
Sonoluminescence	Ultrasounds
Thermoluminescence	Heat
Triboluminescence	Electrostatic and frictional forces

Luminescence in Lanthanides: Lanthanide(III) ions show very unique spectroscopic properties due to shielding of the 4*f* orbitals by the filled 5*s* and 5*p* sub-shells. Lanthanides coordination complexes give very narrow "finger like" emission band which emerges from *f-f* transitions. Each lanthanide ion shows a characteristic absorption and emission spectra and can emit in the entire electromagnetic spectrum from near-UV (Gd(III)), (Eu(III) (red), Tb(III) (green), Sm(III) (orange), Dy(III) (yellow), Tm(III) (blue)), to near-infrared (Yb(III), Nd(III)) (Figure 9).[39]

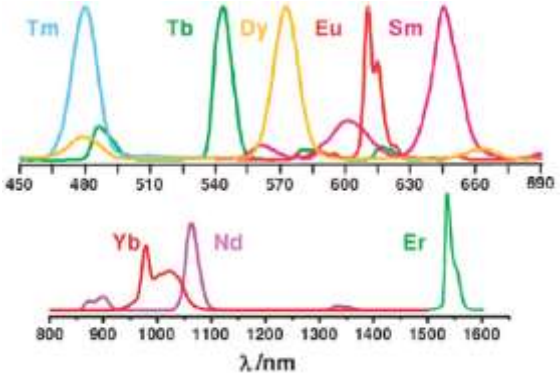

Figure 9. Emission spectra of selected lanthanide(III) ions (adapted from reference 41).

Based on the energy gap between lowest luminescent energy state and highest non-luminescent energy state, lanthanide ions can be categorised into two parts.[42] The first category consists of those lanthanide ions which have low energy gap between transition states and favors radiationless decay and show low luminescence in visible or near infrared region, for example Pr(III), Nd(III), Yb(III), Ho(III), Er(III) and Tm(III). In second category, Lanthanide ions which have high energy gap give strong luminescence in visible range, for example Sm(III), Eu(III), Tb(III) and Dy(III). In case of Gd(III), there is a very large energy gap between excited and ground state - thus excitation and emission features are rarely observed. In case of La(III) and Lu(III) ions, due to empty and completely filled *f* orbitals, respectively, these do not possess any electronic transition.[43] Metal complexes of Yb, Nd and Er ions are less developed because of (i) these lanthanides are less sensitized by the ligands (ii) the energy gap between first excited state and ground state is quite small. MOFs of Tb and Eu are very attractive because of their versatile coordination geometry and high framework stability in water.

2.4 Sensitization Mechanism in Lanthanides

Due to parity forbidded intra-configurational *f-f* transitions by the Laprote selection rule, the lanthanide(III) ions show these transitions with very low molar extinction coefficient ($\varepsilon < 10$ $M^{-1}cm^{-1}$). Therefore, absorption spectra of lanthanide complexes are dominant by ligand-centred absorption bands which are generally very strong and occurs in the UV-vis region. Hence, the forbidden nature of 4*f* transitions resulting into very low extinction coefficient limits the practical applications of the lanthanides. Fortunately, this drawback of lanthanides can be circumvented by using aromatic chromophores[44] which directly bound to the lanthanide(III) centre. Highly intense luminescence from lanthanides can be achieved via an "antenna effect" [45] where the lanthanide ions are sensitized by ligands which have high triplet energies (Figure 10).

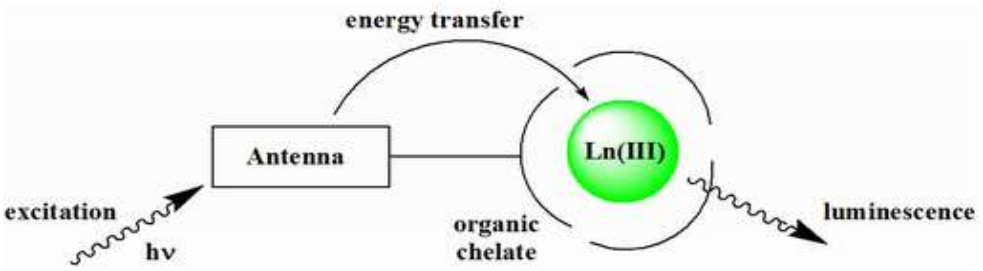

Figure 10. Antenna effect (adapted from reference 46)

Antenna effect works in three steps: light is efficiently absorbed by the ligand from ground state (S_0) to the excited state (S_1) and then energy is transferred to one or several excited state(s) of Ln(III) *via* non-radiative process, and finally Ln(III) emits light efficiently (Figure 11).

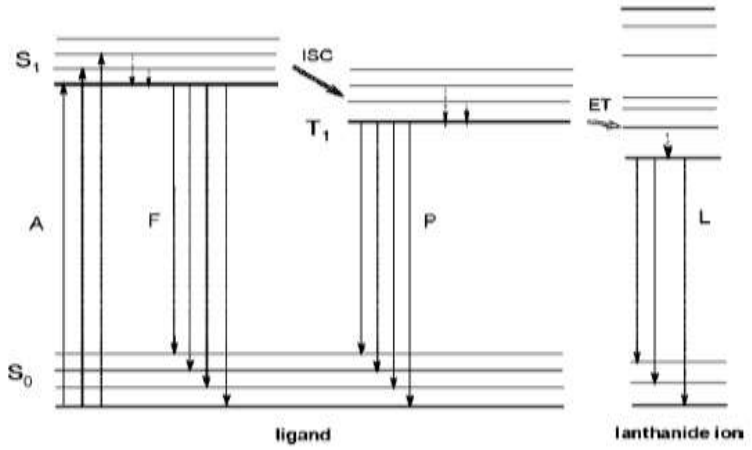

Figure 11. Energy transfer diagram of luminescent lanthanide complexes (adapted from reference 8).

Sensitization of lanthanide emission is achieved when organic aromatic ligand is directly attached to lanthanide centre and it absorbs in the UV-vis spectral region. The energy transfer occurs from triplet state of antenna "ligand" to excited state of Ln(III) ions. To promote the energy transfer, the triplet state of ligand should be higher than the lowest excited state of the lanthanide(III) ion.

The unique luminescence properties in lanthanide(III) ions,[47] i.e., sharp emission, large stoke shift, insensitivity to oxygen and their long excited life-time, which ranges from microsecond (for Nd, Yb) to milliseconds (for Tb, Eu), provoke the evolution of time resolved spectroscopy for application in biological, environmental systems.[48]

2.5 Quenching Process in Lanthanide Complexes

The luminescence from the lanthanide ions not only decays due to radiatative process but can also be quenched through non-radiative decay of the excited state. The electronic excited energy can be dissipated via coupling of the lanthanide energy level with the vibrational modes in the surrounding of the lanthanide ion. The most efficient quencher is the O–H oscillators for the

metal-centred luminescence both in solution and in the solid state. The extent of this quenching is inversely proportional to the energy gap between the emissive state and the ground state of the metal.[49,50] The other quenchers of luminescence are the harmonics of N–H, C–H, and C=O stretching vibrations, but not as O–H oscillators.[50] Polydentate ligands not only increases the stability of the lanthanide complexes in solution but also allows the metal center to be protected from water molecules. Hence, luminescence of the lanthanide based complexes is controlled by the denticity of the ligand. In presence of linkers with low denticity, lanthanides coordinates to solvent molecules resulting in deactivation of the Ln(III) excited states non-radiatatively.

2.5.1 Design of Chromophores for the Sensitization of Lanthanides

For the effective sensitization of the Lanthanide ions, chromophores should fulfill some of the requirements.

1. A chromophore should posses high molar extinction coefficient so that it can absorb energy and transfer to the lanthanide ion efficiently.
2. To reduce the quenching *via* water or solvent molecules, the antenna chromophore should saturate the inner coordination sphere of lanthanide metal ion.
3. The energy levels of the chromophores must be higher than the lowest excited state of the lanthanide ion for effective energy transfer.

The aromatic and heteroaromatic carboxylate based ligands are well known to form infinite polymeric coordination compounds with lanthanides. One of the simplest chromophoric unit is the picolinate moiety, which has been extensively used for the sensitization of lanthanide emitters.[51] Furthermore, the oxophilic character of lanthanide makes carboxylate as best candidates for bridging ligand.[51] A few ligands that have been reported in the literature are shown in Figure 12. The carboxylate based **dpa** ligand (dpa = 2,6-pyridinedicarboxylic acid) with lanthanide is well-studied.[52] An efficient way of assembling four picolinate chromophores into a tetrapodal multidentate ligand **tpaen** that yields ten-coordinate, highly luminescent and water-stable lanthanide complexes, with quantum yields of emission 7% and 45%, respectively, for the Eu(III) and Tb(III) ions.[53] The decadentate ligand **tpabn** gives 1D coordination polymer with Tb(III), where Tb(III) is octa-coordinated with distorted bicapped trigonal prismatic geometry. The reported quantum yield with terbium is 39% and reported lifetime is 1.89 ms.[54] Another picolinate-carboxylate based **bpeda** ligand is reported with Gd(III) ion, which is

applicable as a contrast agent in MRI.[55] Furthermore, **bped** was reported with Sm, Gd, Dy, Nd, Yb, Ho, Lu and La metals by Caravan *et al.*[56]

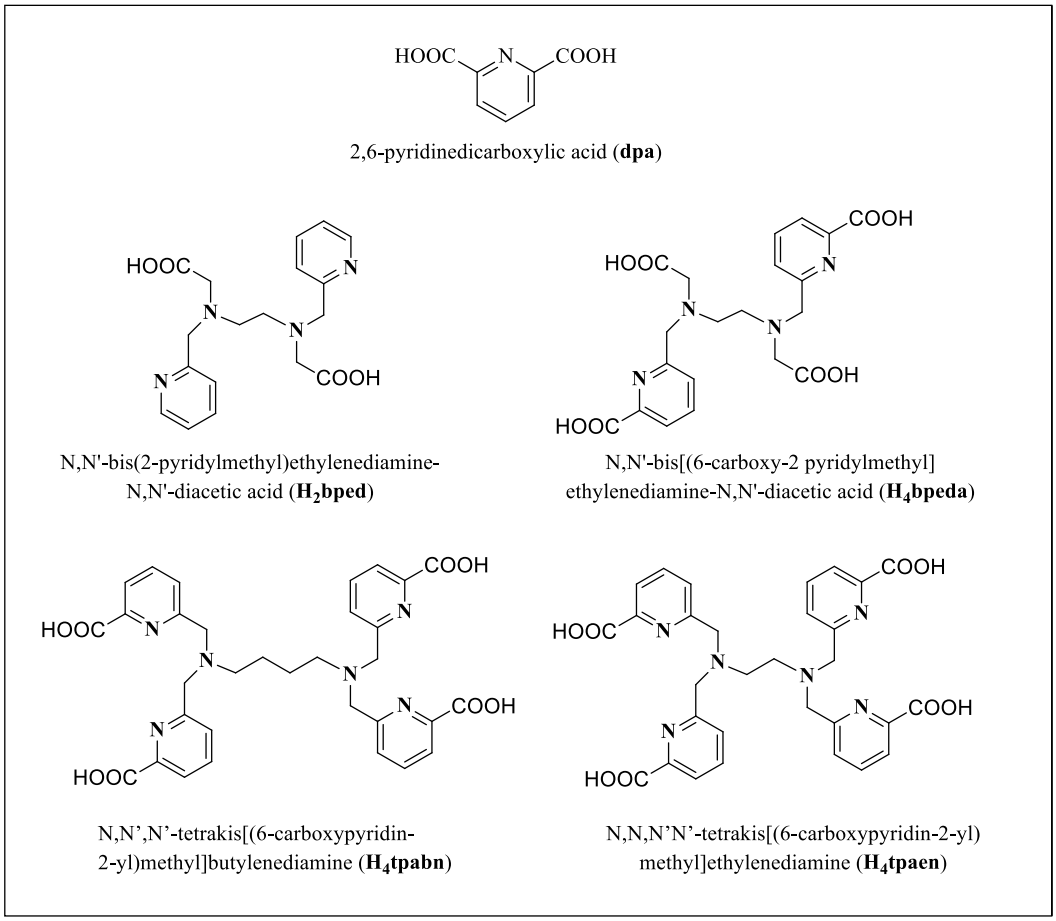

Figure 12. Picolinate based ligands reported in the literature.

Present Work

With an understanding for the choice of ligand and its denticity, in this work a new mixed pyridyl-carboxylate ligand, potassium 2,2'-(butane-1,4-diylbis((pyridin-2-ylmethyl)azanediyl))-diacetate (K_2bpbd), was synthesised. It is an octadentate ligand with two picolinate chromophores and a flexible linear spacer. The picolinate moiety is acting as an antenna, whereas the carboxylate and C_4 spacer directs the dimensionality and the geometry of the self-assembled framework. Purity of the ligand was confirmed by HRMS and ^{1}H NMR data. All these Ln-MOFs were extensively characterized by various spectroscopic techniques (UV-vis and FTIR), elemental analyses, thermogravimetric analysis and powder X-ray diffractometry. Their luminescence property was exploited (all but La complexes show very intense characteristic

luminescence features that confirm the antenna effect of the ligand on the metal centre) to do sensing experiments with various nitro aromatic compounds. Complexes **2**, **4**, **8** and **9** display selective sensing of trinitrophenol (TNP) in water with the best detection limit of 1 ppm for **4**.

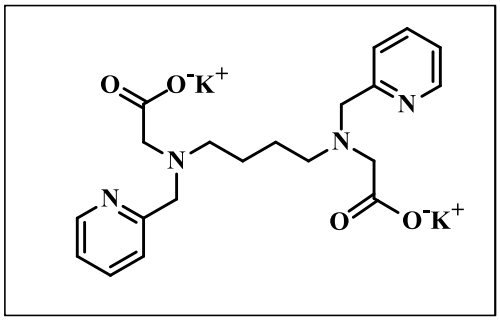

Figure 13. Potassium 2,2'-(butane-1,4-diylbis((pyridin-2-ylmethyl)azanediyl))diacetate (**K_2bpbd**).

Chapter II

Experimental Section

Materials

2-pyridinecarboxaldehyde, 2-Bromoacetic acid, 1,4-diaminobutane, Sodium perchlorate, Potassium hydroxide, Sodium borohydride, Lanthanum nitrate, Neodymium nitrate, Samarium nitrate, Dysprosium nitrate, Terbium nitrate, Lanthanum acetate and Neodymium acetate were obtained from Sigma Aldrich. Lanthanum chloride was obtained from Alfa Aesar. Sodium sulphate was obtained from Merck. Solvents used were of reagent grade and without purified. D_2O was obtained from Sigma Aldrich and $CDCl_3$ was obtained from Merck.

Characterization Techniques

1. Fourier Transform Infrared (FTIR) Spectroscopy: FTIR is a spectroscopic technique used to measure an infrared absorption spectrum. The spectrum gives detail about functional group present in the materials, since distinct functional groups absorb at known characteristic frequencies. Each spectrum was recorded with 16 scans (resolution: 4 cm^{-1}) on a Perkin Elmer Spectrum RX I FT-IR spectrometer using KBr pellets in the range from 4000 – 400 cm^{-1}. The IR spectra also provide binding of anions in the complexes, namely, whether the nitrate, perchlorate and acetate groups were in bound form or in free form and binding of carboxylic groups within a structure.
2. Nuclear Magnetic Resonance (NMR) Spectroscopy: NMR spectroscopy is a physical technique which is used to obtain chemical and structural intuition. It is another kind of absorption spectroscopy, where nuclei of a molecule absorb the energy of radio waves under a strong magnetic field, resulting into transition between nuclear spin states. ^1H NMR spectra were recorded at 400 MHz using Bruker ARX 400 spectrometer, with tetramethylsilane ($Si(CH_3)_4$) as an internal standard. Spinwork software was used to analyse the data.
3. Thermogravimetric Analyses (TGA): Thermogravimetric analysis (TGA) is a method to measure the mass loss/gain in a sample as a function of increasing temperature, under a

controlled atmosphere. It provides a quantitative measurement of the mass loss/gain due to the decomposition, transition, oxidation, etc. Thus, TGA can be used in the determination of the thermal stability and decomposition of a material. Data collection were carried out in a Shimadzu DTG-60H analyser with a heating rate of 10 °C/min under a flow atmosphere of nitrogen from 25–500 °C by using alumina pan.

4. UV-vis Spectroscopy: UV-vis spectroscopy is also known as absorption or reflectance technique. Unlike fluorescence, an absorption measures the transition from ground state to excited state. The UV-vis absorption spectra were obtained on Cary 5000 UV-Vis-NIR spectrophotometer from range 200-800 nm.
5. Elemental Analyses: Elemental analysis was used to explicate the empirical formula of the complexes. CHN used to determine the percentage amounts of carbon, hydrogen and nitrogen in the material. C, H, and N analyses were performed on Leco, TrueSpec, Micro CHNS analyzer. Typical mass of a sample was 2 mg.
6. Powder X-ray Diffraction (PXRD): PXRD is the analytical technique which is used for characterize crystalline materials. It is used in determine lattice parameters, phase identification, phase transitions, size and strain broadening. PXRD patterns were collected in the $2\theta = 3-50°$ range with a scanning speed of 5° per minute with interval 0.02°, on a Rigaku Ultima IV diffractometer using parallel beam geometry, sample rotation (120 rpm) attachment and DTex Ultra detector.
7. Photoluminescence: Photoluminescence is an absorption/emission technique where emission transitions occur from excited state to ground state. Luminescence spectra for the solid samples were recorded by a Shimadzu RF-5301 PC spectrofluorophotometer. The photomultiplier tube voltage was 250 V the detector was photomultilier and the source was xenon lamp, while the slit widths of excitation and emission spectra were 5 nm.
8. Scanning Electron Microscopy (SEM): The scanning electron microscope (SEM) scans the surface of the material via focused beam of high energy electrons. The electrons interact with the atoms at the solid surface and give different kind of the signals. The signals include secondary electrons, backscattered electrons, diffracted backscattered electrons, X-rays, etc. The signals (secondary electrons and backscattered electrons)

derive from electron-sample interactions shows the information regarding the morphology, chemical composition. The SEM was done on JEOL JSM-7600F.

Preparation of Ligand (K_2bpbd). Step I: 2-pyridinecarboxaldehyde (3.8 mL, 40 mmol) was dissolved in 5 mL of methanol. To this solution, 1,4-diaminebutane (2 mL, 20 mmol) was added dropwise at 0°C with continuous stirring, the reaction mixture was stirred for 4 h at room temperature followed by addition of sodium borohydride at 0° C and it was again stirred for 12h. After the stirring was stopped, the solvent was evaporated under reduced pressure, followed by extraction of the compound using DCM and H_2O, DCM layer was washed with water (3 x 2 ml). The DCM layer was collected in a separate conical flask, dried with anhydrous sodium sulphate for half an hour followed by filtration. The solvent evaporation was evaporated to dryness. A yellow colored oily product (**bpbn**) was obatined. Yield: 4.4 g (97.8%). ^{1}H NMR ($CDCl_3$) δ: 8.53 (d, 2H), 7.62 (t, 2H), 7.30 (m, 2H), 7.13 (d, 2H) 3.97 (s, 4H), 2.66 (s, 4H), 2.59 (t, 2H), 1.59 (t, 4H).

Step II: Bromoacetic acid (830 mg, 6 mmol) was dissolved in 5 mL water. A solution of potassium hydroxide (349 mg, 6 mmol) was dissolved in 5 mL of water and added dropwise to the bromoacetic acid solution and stirred for 30 minutes. The above solution was added to the solution of Compund **bpbn** (830 mg, 3 mmol) was dissolved in 5 mL water and added dropwise at 0°C with continuous stirring. After half an hour, a solution of KOH (354 mg, 6 mmol) in 5 mLwater was added to the above reaction mixture at 0°C and the resulting reaction mixture was further stirred for 96 h. After the stirring was over, solvent was evaporated under reduced pressure. To the crude product obtained, potassium bromide was separated out by filtration and filtrate was washed with methanol and evaporated to the dryness. To the semi-solid product obtained after evaporating methanol, 5mL acetonitrile was added, and dried under high vacuum to get the desired product. The product obtained was off-white solid. Yield: 800 mg (60%). MS (ESI-TOF): m/z calc. for $[(C_{20}H_{26}N_6O_4)H]^+$, 387.198; found, 387.187.^{1}H NMR (D_2O) δ: 8.34 (d, 2H), 7.75 (m, 2H), 7.40 (m, 2H), 7.25 (d, 2H), 3.83 (s, 4H), 3.14 (s, 4H), 2.51 (s, 4H), 1.33 (s, 4H). Selected FTIR peaks (KBr, cm^{-1}): 3434 (b,O-H), 1592 (s, COO_{asym}), 1402 (s, COO_{sym}), 768 (s).

Preparation of Metal Complexes

{[La(bpbd)(H_2O)$_2$(NO_3)]·7H_2O}$_n$ (1). La(NO_3)$_3$·6H_2O (20 mg, 0.046 mmol) and K_2bpbd (22 mg, 0.046 mmol) was added in 2 mL of water. The reaction mixture was stirred for 4 h at ambient conditions. A white solid product was obtained via filtration, washed with water and air dried. Yield: 17 mg (50 %). Anal. Calc. for $C_{20}H_{42}N_5O_{16}La$ (MW 747.48) C, 32.41; H, 5.66; N, 9.37. Found C, 33.09; H, 5.41; N, 8.59. Selected FTIR peaks (KBr, cm^{-1}): 3413 (b,O-H), 1580 (s, COO_{asym}), 1384 (s, NO_3), 1408 (s, COO_{sym}), 766 (s).

{[Nd(bpbd)(H_2O)$_2$(NO_3)]·7H_2O}$_n$ (2). Method A: Nd(NO_3)$_3$·6H_2O (20 mg, 0.046 mmol) was added to a solution of K_2bpbd (21 mg, 0.046 mmol) in 2 mL of water. The reaction mixture was stirred for 4 h at room temperature. A white solid product was obtained via filtration, washed with water and air dried. Yield: 21 mg (61%). Anal. Calc. for $C_{20}H_{42}N_5O_{16}Nd$ (MW 753) C, 31.91; H, 5.62; N, 9.30. Found C, 32.15; H, 5.59; N, 8.59. Selected FTIR peaks (KBr, cm^{-1}): 3418 (b, O-H), 1584 (s, COO_{asym}), 1384 (s, NO_3), 1328 (s, COO_{sym}), 766 (s).

Method B: Nd(NO_3)$_3$·6H_2O (20 mg, 0.046 mmol) and K_2bpbd (21 mg, 0.046 mmol) in 2 mL of water was sealed in a 5 mL Teflon-lined stainless steel vessel. Using a programmable oven, it was heated under autogenous pressure at 120 °C for 1 day and then cooled to RT at 10 °C/h. A white solid product was obtained which was filtered, washed with water and air dried. Yield: 16 mg (50%). Anal. Calc. for $C_{20}H_{42}N_5O_{16}Nd$ (MW 753) C, 31.91; H, 5.62; N, 9.30. Found C, 31.82; H, 5.80; N, 8.11. Selected FTIR peaks (KBr, cm^{-1}): 3418 (b, O-H), 1584 (s, COO_{asym}), 1384 (s, NO_3), 1328 (s, COO_{sym}), 766 (s).

{[Sm(bpbd)(H_2O)$_2$(NO_3)]·7H_2O}$_n$ (3). Sm(NO_3)$_3$·6H_2O (20 mg, 0.045 mmol) was added to a solution of, K_2bpbd (21 mg, 0.045 mmol) in 2 mL of water. The complex was precipitated out after 4 h of stirring. A white solid product was obtained via filtration, washed with water and air dried. Yield: 17 mg (50%). Anal. Calc. for $C_{20}H_{42}N_5O_{16}Sm$ (MW 758.93) C, 31.65; H, 5.58; N, 9.23. Found C, 32.10; H, 5.49; N, 8.70. Selected FTIR peaks (KBr, cm^{-1}): 3434 (b, O-H), 1587 (s, COO_{asym}), 1384 (s, NO_3), 1410 (s, COO_{sym}), 766 (s).

{[Tb(bpbd)(H_2O)$_2$(NO_3)]·5H_2O}$_n$ (4). Tb(NO_3)$_3$·6H_2O (20 mg, 0.044 mmol) and K_2bpbd (21 mg, 0.046 mmol) was added in 2 mL of water. The reaction mixture was stirred for 4 h at ambient conditions. A white solid product was obtained via filtration, washed with water and air dried. Yield: 10 mg (30%). Anal. Calc. for $C_{20}H_{28}N_5O_9Tb$ (MW 731.47) C, 32.84; H, 5.24; N,

9.57. Found C, 31.66; H, 4.77; N, 6.79. Selected FTIR peaks (KBr, cm^{-1}): 3426 (b, O-H), 1596 (s, COO_{asym}), 1384 (s, NO_3), 1409 (s, COO_{sym}), 767 (s).

{[Dy(bpbd)(H_2O)$_2$(NO_3)]·5H_2O}$_n$ (5). $Dy(NO_3)_3·6H_2O$ (20 mg, 44 mmol) was added to a solution of K_2bpbd (21 mg, 44 mmol) in water (2 mL). The resulting solution was stirred at room temperature for 4 h. A white solid product was obtained via filtration, washed with water and air dried. Yield: 7 mg (21%). Anal. Calc. for $C_{20}H_{28}N_5O_9Dy$ (MW 735.03) C, 32.68; H, 5.21; N, 9.53. Found C, 31.07; H, 4.38; N, 7.23. Selected FTIR peaks (KBr, cm^{-1}): 3418 (b, O-H), 1604 (s, COO_{asym}), 1384 (s, NO_3), 1408 (s, COO_{sym}), 766 (s).

{[La(bpbd)(H_2O)$_2$(OAc)]·5H_2O}$_n$ (6). $La(OAc)_3·6H_2O$ (20 mg, 46 mmol) was added to a solution of K_2bpbd (21 mg, 46 mmol) in water (2 mL). After the reaction mixture was stirred at room temperature for 4 hour, the resulting mixture was filtered. A white solid product was obtained via filtration, washed with water and air dried. Yield: 11 mg (33%). Anal. Calc. for $C_{22}H_{42}N_4O_{13}La$ (MW 708.49) C, 37.30; H, 5.83; N, 7.91. Found C, 37.74; H, 5.05; N, 7.07. Selected FTIR peaks (KBr, cm^{-1}): 3424 (b, O-H), 1572 (s, COO_{asym}), 1412 (s, COO_{sym}), 763 (s).

{[La(bpbd)(H_2O)$_2$(Cl)]·5H_2O}$_n$ (7). $LaCl_3·7H_2O$ (20 mg, 0.054 mmol) was added to a solution of K_2bpbd (25 mg, 0.054 mmol) in water (2 mL). The solution was stirred at room temperature for 4 h. A white solid product was obtained via filtration, washed with water and air dried. Yield: 15 mg (42 %). Anal. Calc. for $C_{20}H_{38}N_4O_{11}ClLa$ (MW 685) C, 35.07; H, 5.59; N, 8.18. Found C, 36.42; H, 5.55; N, 8.03. Selected FTIR peaks (KBr, cm^{-1}): 3409 (b, O-H), 1597 (s, COO_{asym}), 1411 (s, COO_{sym}), 764 (s).

{[Nd(bpbd)(H_2O)$_2$(OAc)]·7H_2O}$_n$ (8). $Nd(OAc)_3·6H_2O$ (20 mg, 46 mmol) was added to a solution of K_2bpbd (21 mg, 46 mmol) in water (2 mL). The reaction mixture was stirred at room temperature for 4 h. A white solid product was obtained via filtration, washed with water and air dried. Yield: 16 mg (48%). Anal. Calc. for $C_{22}H_{45}N_4O_{15}Nd$ (MW 749.85) C, 35.24; H, 6.05; N, 7.47. Found C, 33.39; H, 5.18; N, 6.93. Selected FTIR peaks (KBr, cm^{-1}): 3411 (b, O-H), 1570 (s, COO_{asym}), 1410 (s, COO_{sym}), 767 (s).

{[Nd(bpbd)(H_2O)$_2$(ClO_4)]·5H_2O}$_n$ (9). $Nd(OAc)_3·6H_2O$ (20 mg, 0.046 mmol), K_2bpbd (21 mg, 0.046 mmol) and sodium perchlorate was added in a 2 mL of water. The complex **9** was precipitated out after 4 h of stirring. A white solid product was obtained via filtration, washed with water and air dried. Yield: 30 mg (85%). Anal. Calc. for $C_{20}H_{38}N_4O_{11}ClNd$ (MW 754.23) C,

31.85; H, 5.08; N, 7.43 Found: C, 31.07; H, 4.55; N, 7.05. Selected FTIR peaks (KBr, cm^{-1}): 3418 (w), 1584 (s, COO_{asym}), 1410 (s, COO_{sym}), 1089 (s), 1128 (s, ClO_4), 766 (s).

Sensing Experiments

Fluorescence spectra were recorded in the solution state (water or DMSO) or as a slurry in DMSO. To carry out the sensing studies, 10 μL of a 2 mM solution of the analyte was added to 2 mL of a 0.7 mM solution of the sensor (metal complex).

Chapter III

Results and Discussion

Synthesis of Ligand. K_2bpbd was obtained in two steps from commercially available 2-pyridinecarboxaldehyde, 2-bromoacetic acid and 1,4-diaminobutane in an overall yield of 60% (see Scheme I below). In the first step, the condensation of aldehyde and diamine in a ratio of 2:1 resulted in the formation of a Schiff base which was reduced by sodium borohydride in single pot to yield the intermediate bpbn in 98% yield. The ^{1}H NMR spectrum confirmed the formation of bpbn (as shown in Figure 14)**.** In the second step, bpbn was reacted with the potassium salt of bromoacetic acid in water (preformed with 2 eqv. of potassium hydroxide) to generate K_2bpbd. Its HRMS data is consistent with its formula. K_2bpbd was further characterized by ^{1}H NMR and FTIR spectroscopy (as shown in Figures 15 and 16, respectively). For K_2bpbd, a peak at 1592 cm^{-1} corresponds to the asymmetric stretching frequency of carboxylate, a peak at 1402 cm^{-1} correspond to the symmetric stretching of carboxylate and a peak at 768 cm^{-1} corresponds to the C-H stretching near nitrogen of pyridine.

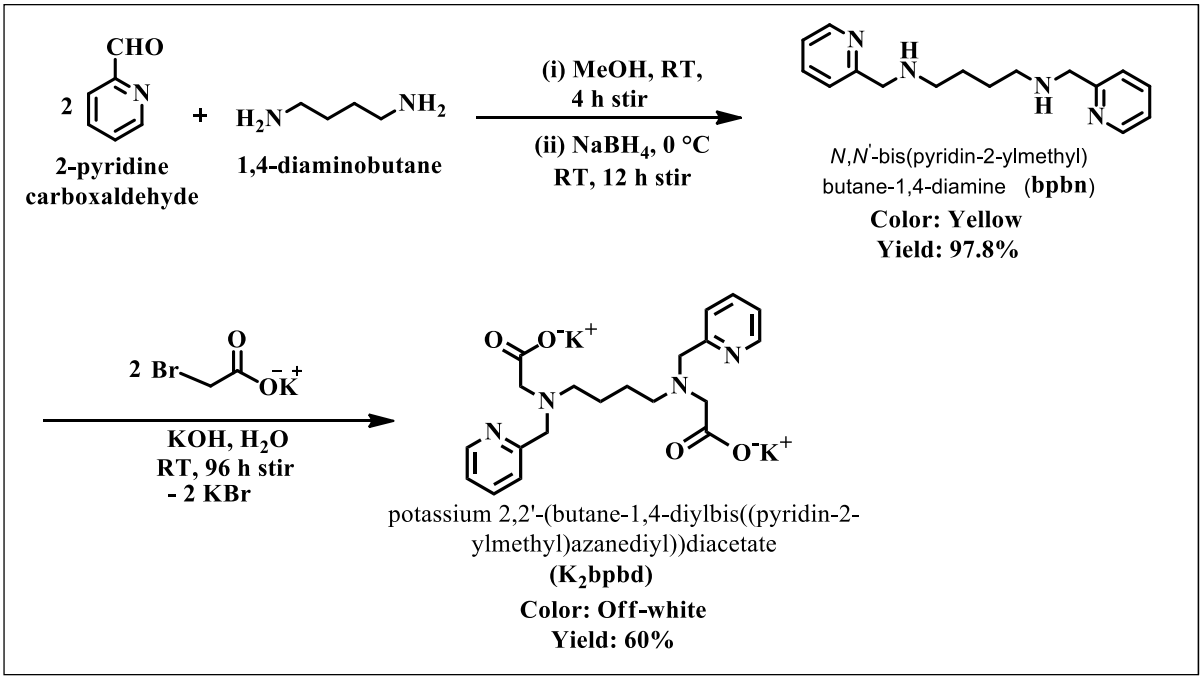

Scheme I. Synthesis of K_2bpbd.

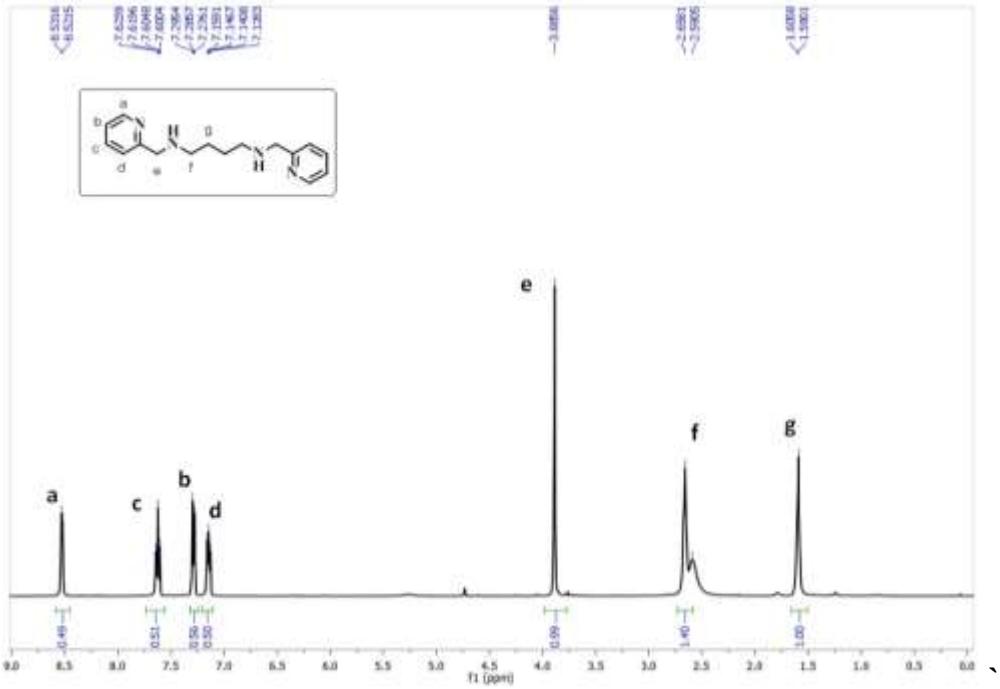

Figure 14. ^{1}H NMR of **bpbn** in $CDCl_3$.

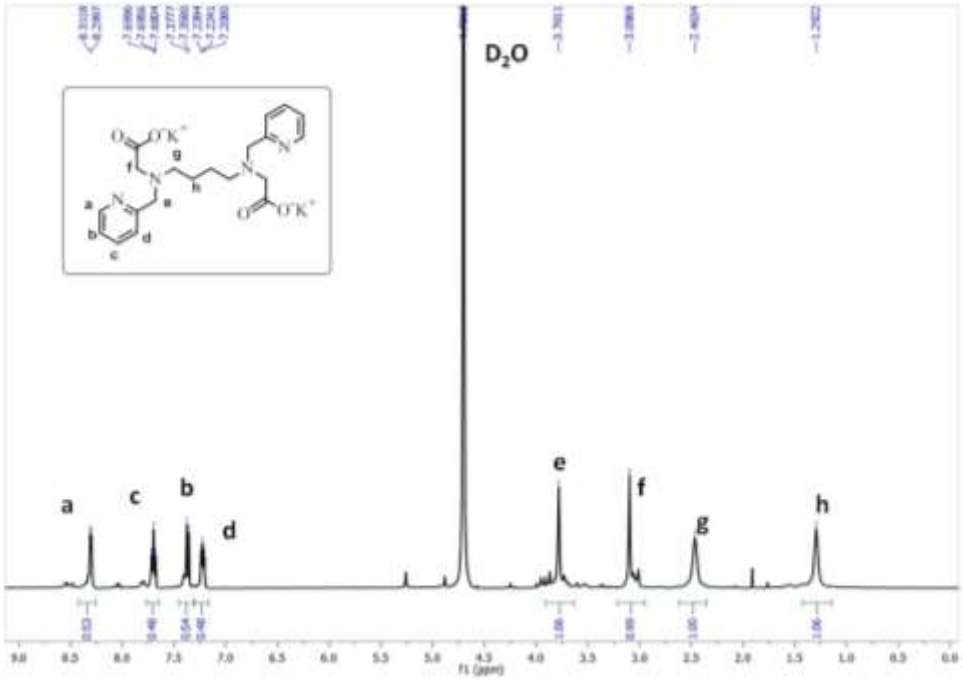

Figure 15. ^{1}H NMR of **K_2bpbd** in D_2O.

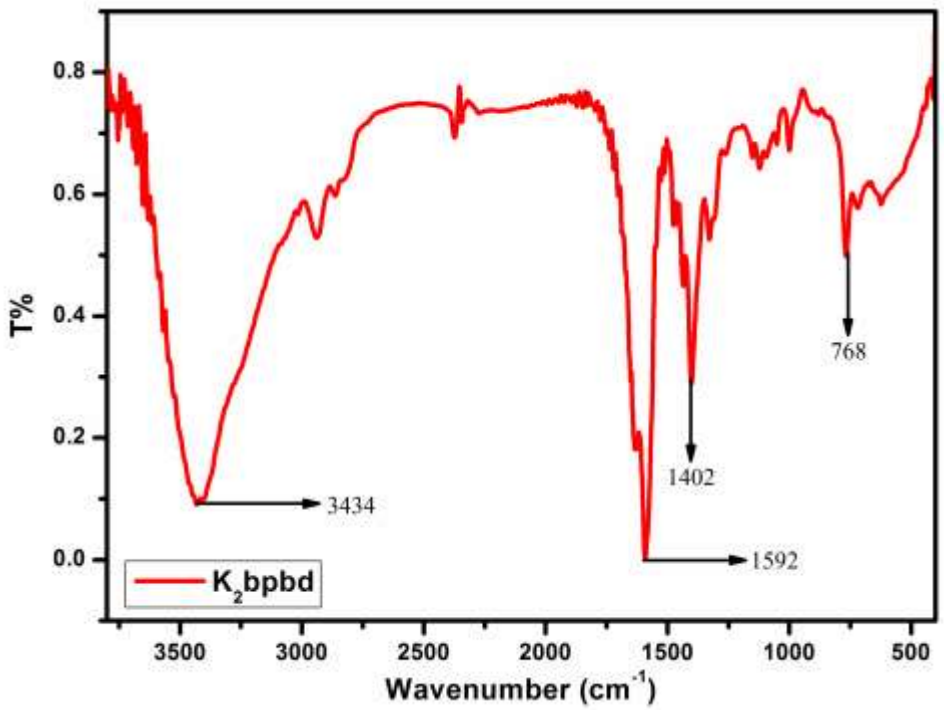

Figure 16. FTIR spectrum of **K_2bpbd**.

Synthesis of Lanthanide Complexes. Lanthanide complexes (**1-8**) were synthesized by reacting the corresponding lanthanide salt and the ligand in a 1:1 ratio in water by the conventional one-pot synthesis at room temperature while for compound **9** the acetate was exchanged with perchlorate by adding sodium perchlorate. All these complexes are white in color.

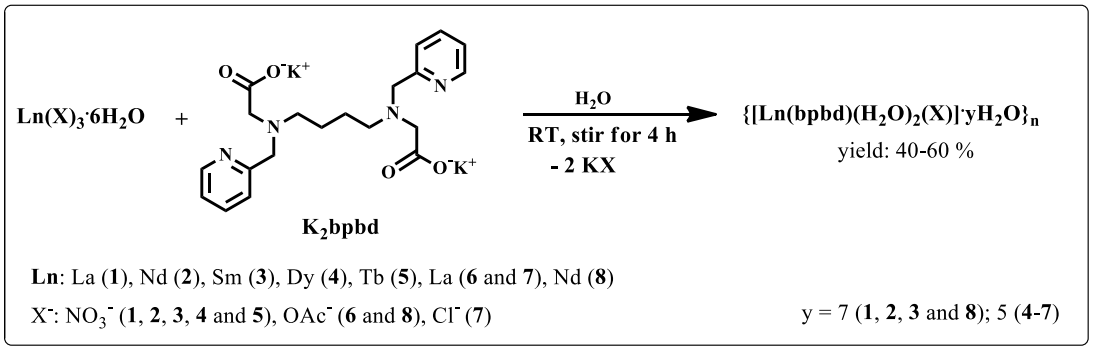

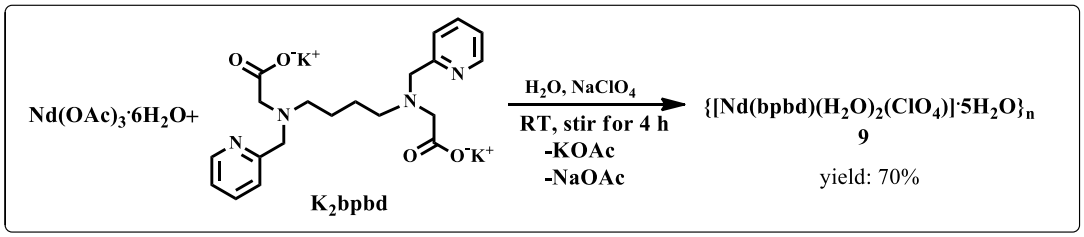

Scheme II. Synthesis of Metal Complexes.

FTIR Spectroscopy

FTIR spectra were collected for all the synthesized compounds using KBr pellets on Perkin Elmer Spectrum RX I FTIR spectrometer in the 4000-400 cm^{-1} range. FTIR spectra for metal complexes **1**-**5** (Figures 17-21) are very similar and show strong bands for asymmetric and symmetric stretching vibrations of the dicarboxylate group at ~1590 and ~1410 cm^{-1}. The difference between asymmetric and symmetric stretching is around 175 cm^{-1} which indicates that in **1**-**5** the carboxylate binds with Lanthanides in bidentate chelating fashion (see Table 2). A peak at 1384 cm^{-1} in **1-5** corresponds to the nitrate binding in monodentate fashion to the metal centre (see Table 3). A peak at 3422-3446 cm^{-1} shows the O-H stretching frequency for coordinated water. On the other hand, compounds **6** and **8** show the characteristic features of a coordinated acetate group, which is missing in compound **7**, in addition to other features from the ligand (see Figures 22-24). For compound **9,** strong peaks at 1089 and 1121 cm^{-1} shows the presence of uncoordinated perchlorate ion (see Figure 25).

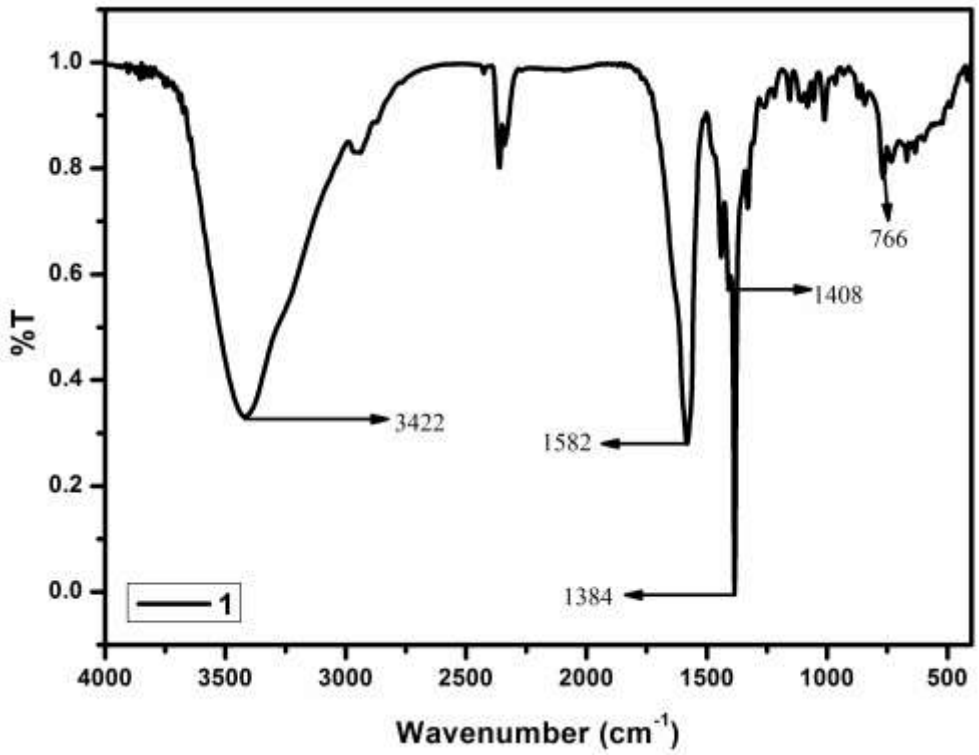

Figure 17. FTIR Spectrum of $\{[La(bpbd)(H_2O)_2(NO_3)]\cdot 7H_2O\}_n$ (**1**).

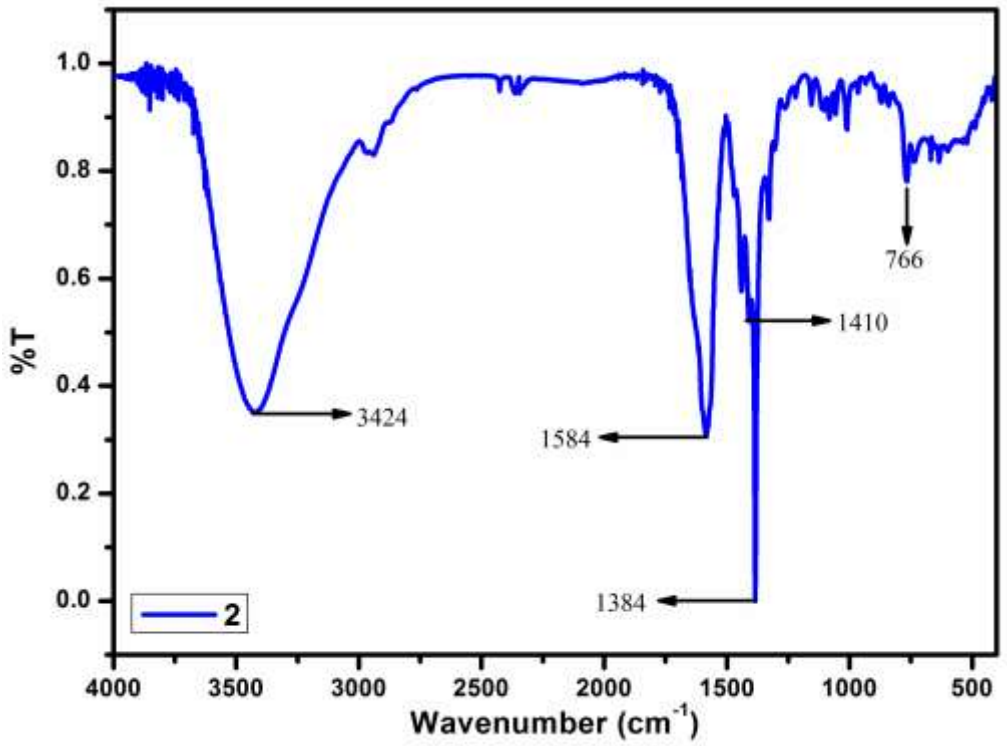

Figure 18. FTIR Spectrum of $\{[Nd(bpbd)(H_2O)_2(NO_3)]\cdot 7H_2O\}_n$ (**2**).

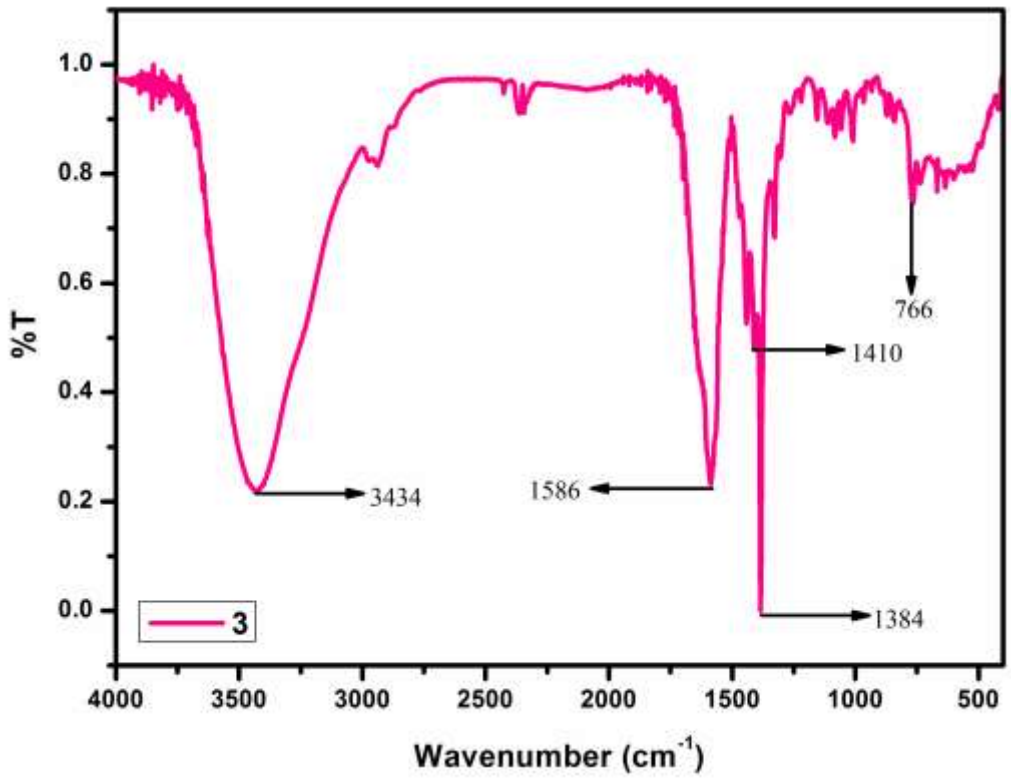

Figure 19. FTIR Spectrum of $\{[Sm(bpbd)(H_2O)_2(NO_3)]\cdot 7H_2O\}_n$ (**3**).

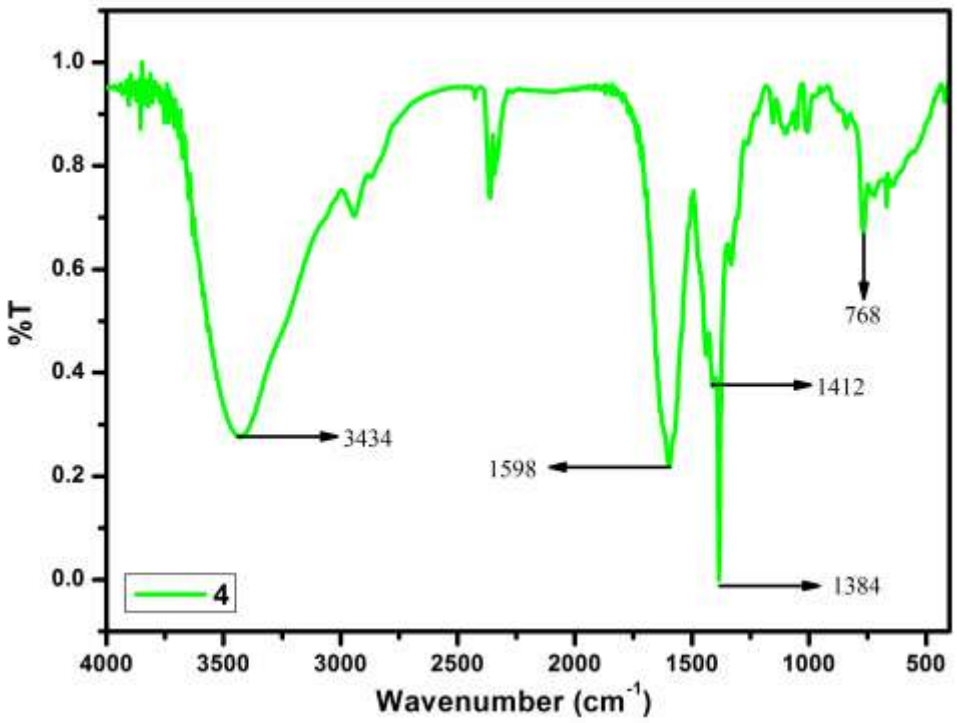

Figure 20. FTIR Spectrum of {[Tb(bpbd)(H_2O)$_2$(NO_3)]·5H_2O}$_n$ (**4**).

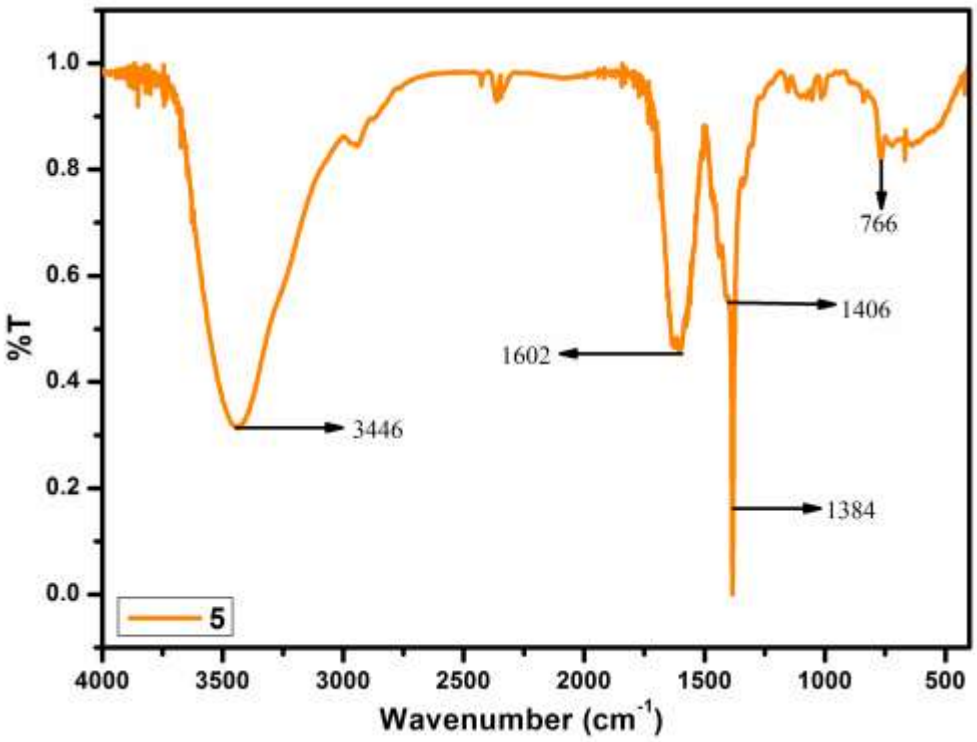

Figure 21. FTIR Spectrum of {[Dy(bpbd)(H_2O)$_2$(NO_3)]·5H_2O}$_n$ (**5**).

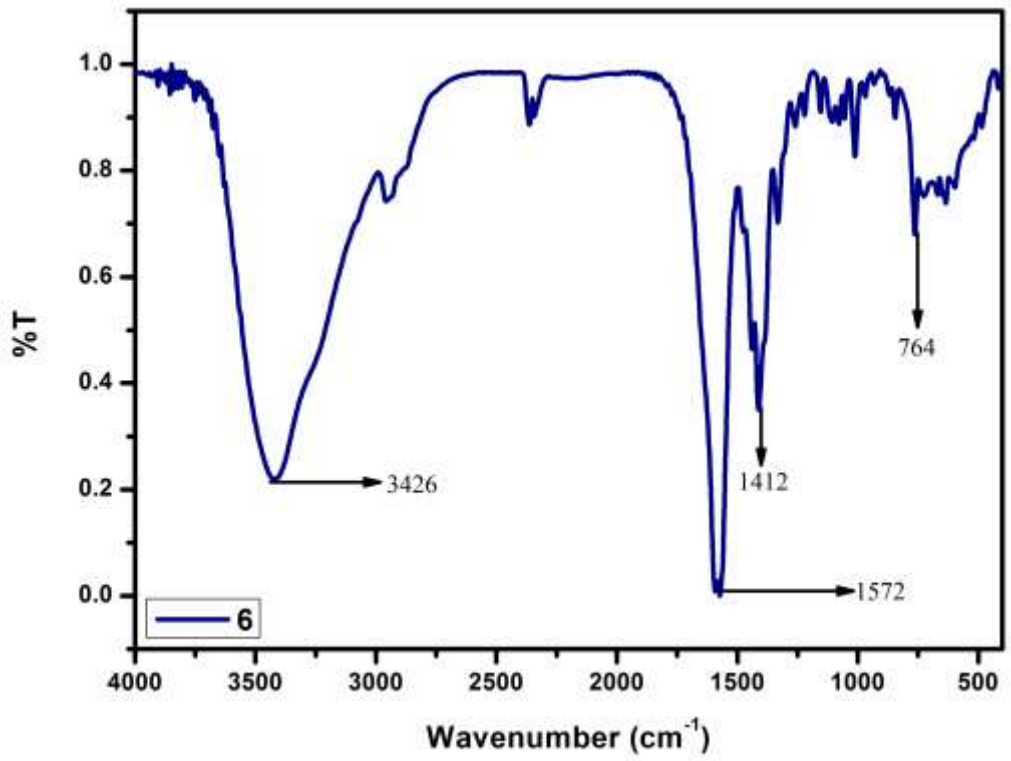

Figure 22. FTIR Spectrum of $\{[La(bpbd)(H_2O)_2(OAc)]\cdot 5H_2O\}_n$ (**6**).

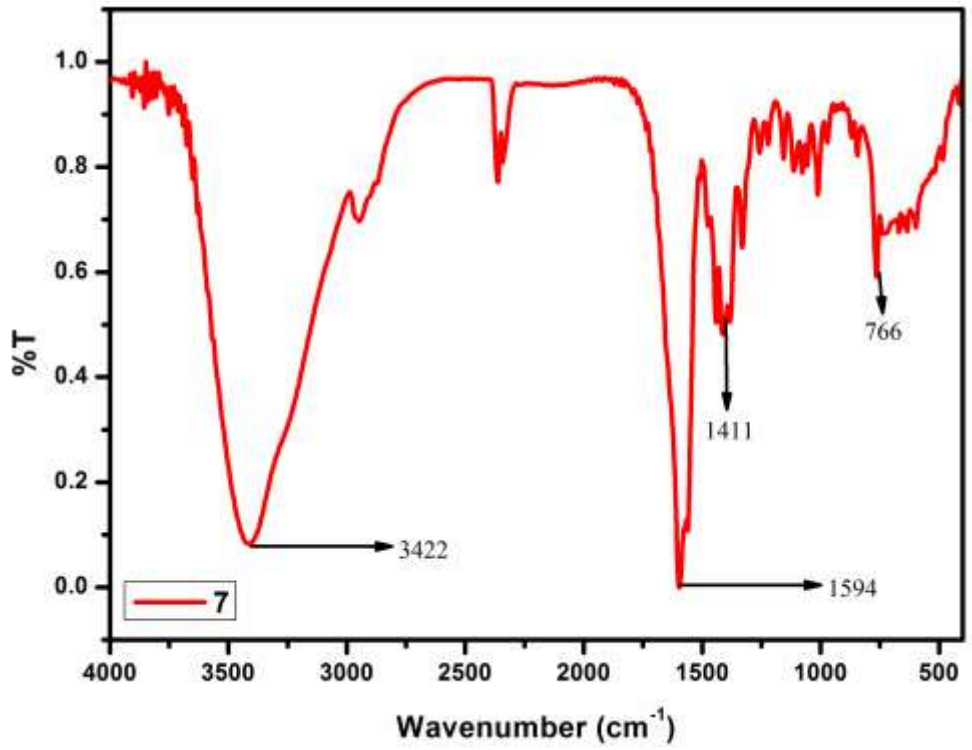

Figure 23. FTIR Spectrum of $\{[La(bpbd)(H_2O)_2(Cl)]\cdot 5H_2O\}_n$ (**7**).

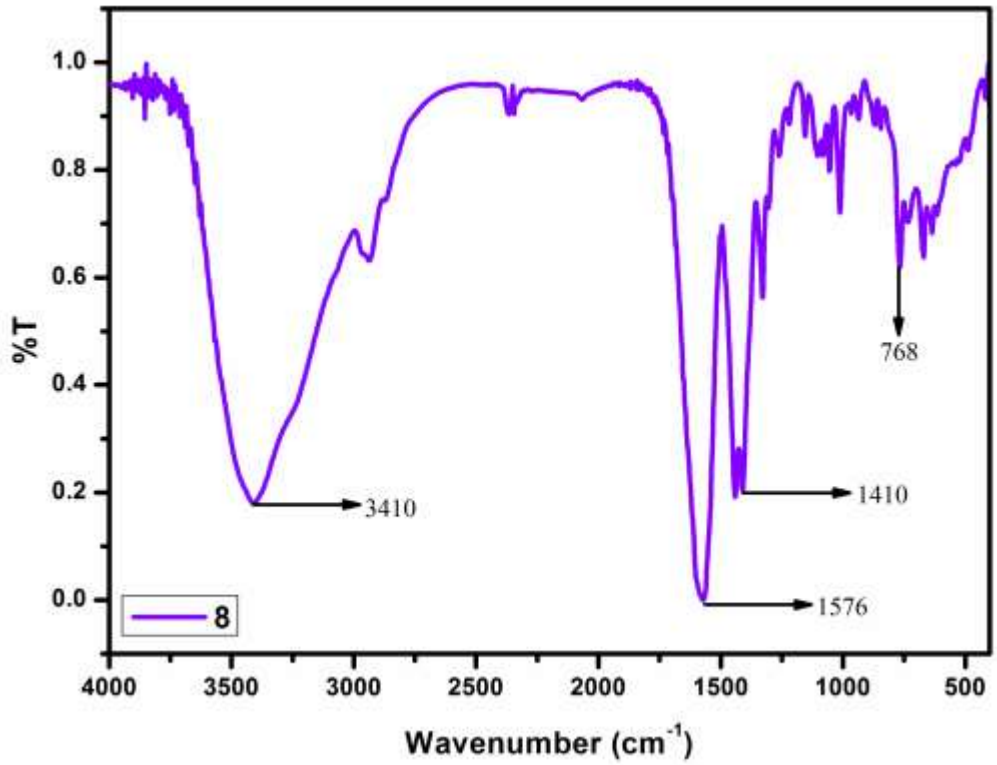

Figure 24. FTIR Spectrum of $\{[Nd(2\text{-}bpbd)(H_2O)_2(OAc)]\cdot 7H_2O\}_n$ (**8**).

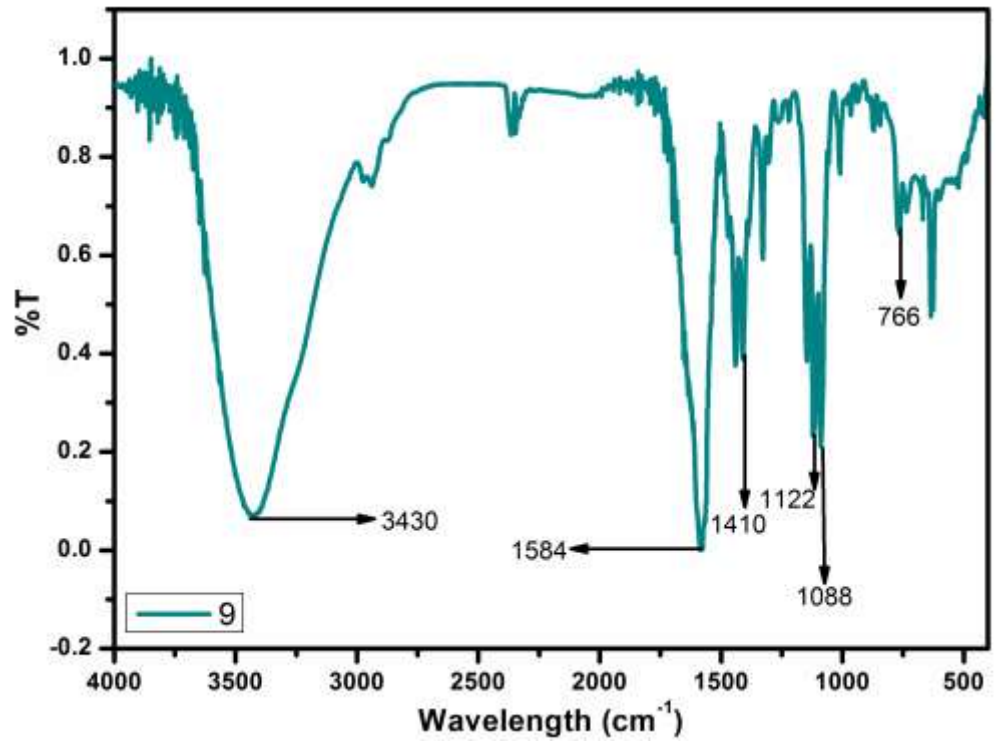

Figure 25. FTIR Spectrum of $\{[Nd(bpbd)(H_2O)_2(ClO_4)]\cdot 5H_2O\}_n$ (**9**).

In order to utilize the FTIR data of these metal complexes for their structural characterization, the binding of the carboxylate groups in the bpbd ligand and the nitrate anions are analyzed. Based on data listed in Tables 2 and 3, chelating bidentate binding mode of the carboxylate and monodentate binding mode of nitrate.

Table 2. Carboxylate stretching frequencies and binding modes with the metal centre**.**

Carboxylate binding mode				
Metal Complexes	ν_{asym} (cm^{-1})	ν_{symm} (cm^{-1})	$\Delta\nu$ (cm^{-1})	Binding mode
$\{[La(bpbd)(H_2O)_2(NO_3)]\cdot 7H_2O\}_n$ (**1**)	1580	1408	172	Chelating bidentate
$\{[Nd(bpbd)(H_2O)_2(NO_3)]\cdot 7H_2O\}_n$ (**2**)	1584	1409	175	Chelating bidentate
$\{[Sm(bpbd)(H_2O)_2(NO_3)]\cdot 7H_2O\}_n$ (**3**)	1586	1410	176	Chelating bidentate
$\{[Tb(bpbd)(H_2O)_2(NO_3)]\cdot 5H_2O\}_n$ (**4**)	1595	1409	186	Chelating bidentate
$\{[Dy(bpbd)(H_2O)_2(NO_3)]\cdot 5H_2O\}_n$ (**5**)	1604	1408	196	Chelating bidentate
$\{[La(bpbd)(H_2O)_2(OAc)]\cdot 5H_2O\}_n$ (**6**)	1595	1412	183	Chelating bidentate
$\{[La(bpbd)(H_2O)_2(Cl)]\cdot 5H_2O\}_n$ (**7**)	1597	1411	186	Chelating bidentate
$\{[Nd(bpbd)(H_2O)_2(OAc)]\cdot 7H_2O\}_n$ (**8**)	1570	1411	159	Chelating bidentate
$\{[Nd(bpbd)(H_2O)_2(ClO_4)]\cdot 5H_2O\}_n$ (**9**)	1584	1410	174	Chelating bidentate

Table 3. Nitrate stretching frequencies and binding mode with the metal centre.

Nitrate binding mode		
Metal Complexes	v (cm^{-1})	Binding mode
$\{[La(bpbd)(H_2O)_2(NO_3)]\cdot 7H_2O\}_n$ (**1**)	1384, 1011	Monodentate
$\{[Nd(bpbd)(H_2O)_2(NO_3)]\cdot 7H_2O\}_n$ (**2**)	1384, 1010	monodentate
$\{[Sm(bpbd)(H_2O)_2(NO_3)]\cdot 7H_2O\}_n$ (**3**)	1384, 1010	monodentate
$\{[Tb(bpbd)(H_2O)_2(NO_3)]\cdot 5H_2O\}_n$ (**4**)	1384, 1005	monodentate
$\{[Dy(bpbd)(H_2O)_2(NO_3)]\cdot 5H_2O\}_n$ (**5**)	1384, 1015	monodentate

UV-Visible Spectroscopy

In all UV-vis spectra, the absorbance bands were dominated by a transition within the ligand at 262 nm (Figure 26).

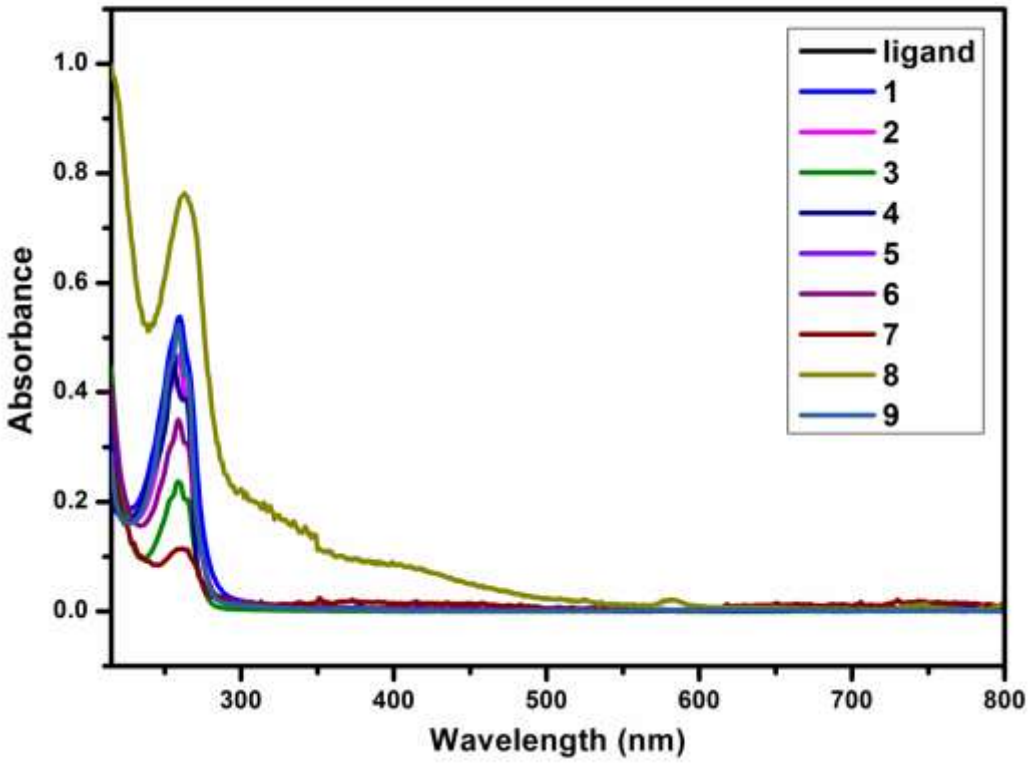

Figure 26. Absorbance spectra of **K_2bpbd** and compounds **1-9**.

Thermogravimetric Analysis

TGA profiles of **1-8** are shown in Figures 27-30. Complexes **1-3**, **4**, **5** and **8** showed similar thermal stability. TGA profile of **2**, synthesized at room temperature (25 ^{o}C) and hydrothermal (120 °C) are showing the formation of same products (see Figure 28). Complex **6** shows continuous weight loss (see Figure 30). Thermogravimetric isotherm curve obtained for complex **1-3** and **8** prove the two molecules of water are present as coordinated and seven are present as lattice water molecules. From room temperature (25 °C) to about 100 °C, all isostructural compounds (**1**, **2**, **3** and **8**) lose approximately 13% of their initial weight. This weight loss corresponds to the loss of lattice water molecules. The complexes **1**, **2**, **3** and **8** and **7** started decomposition after 220 °C (Figure 27 and 30). TGA analysis of compound **9** cannot be performed because of the presence of a perchlorate ion.

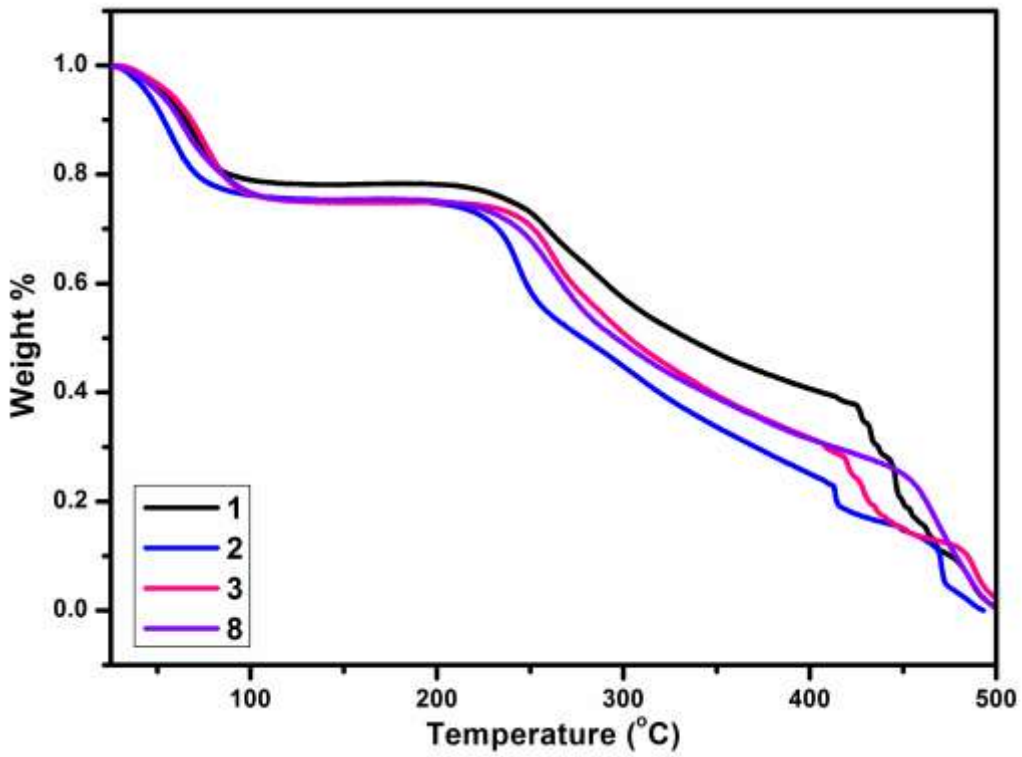

Figure 27. TGA Profile of Complex **1**, **2**, **3** and **8**.

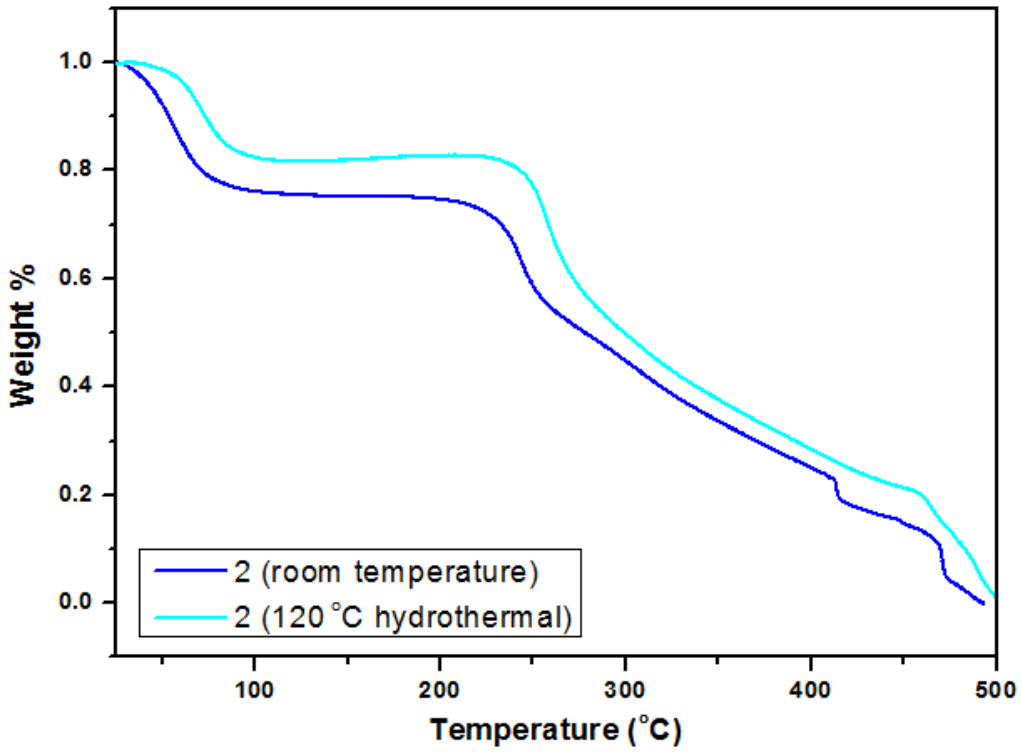

Figure 28. TGA Profile of complex **2** synthesized at hydrothermal and RT.

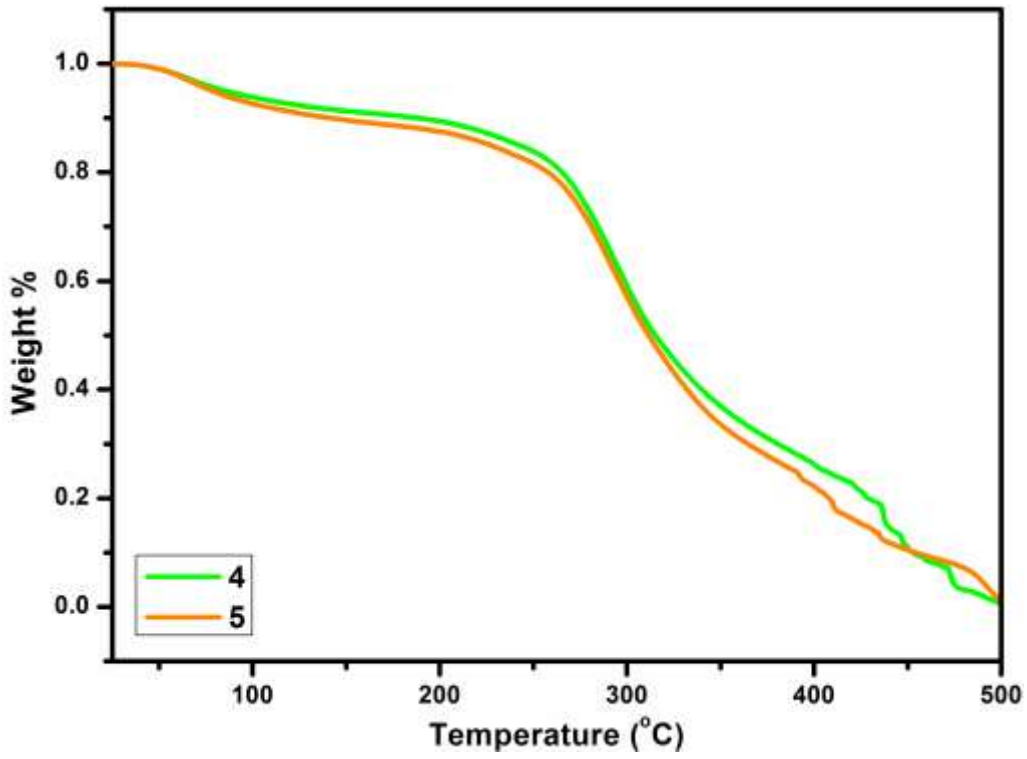

Figure 29. TGA Profile of complex **4** and **5**.

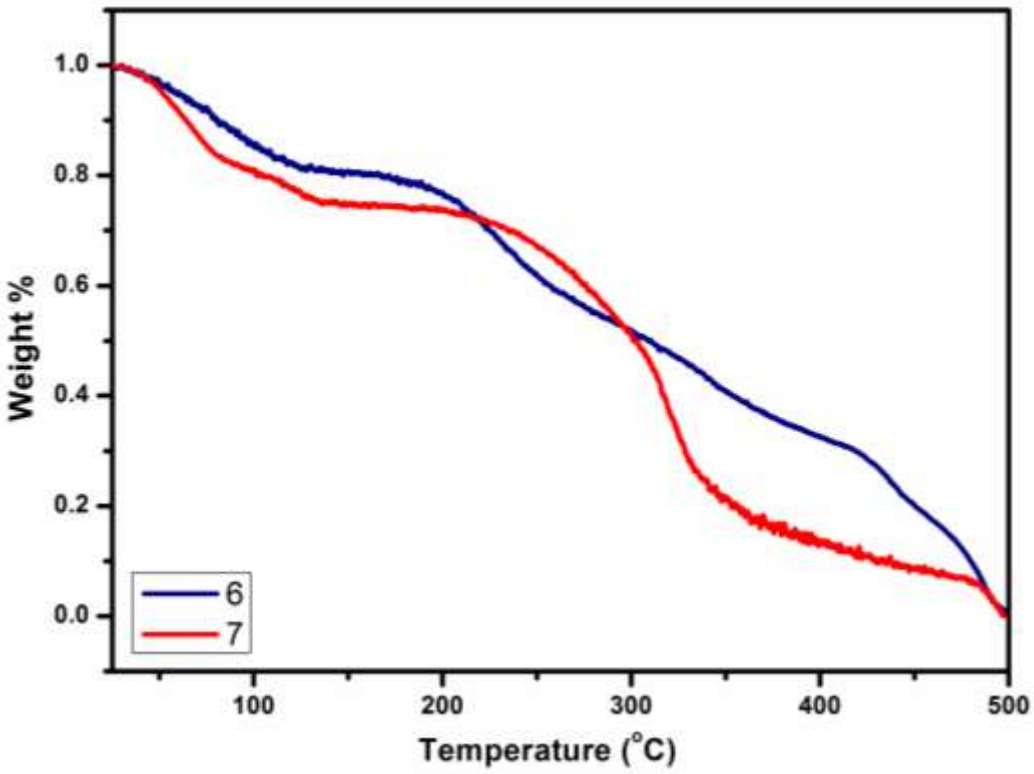

Figure 30. TGA Profile of complex **6** and **7**.

Powder X-ray Diffraction Analysis

Powder data was collected on Rigaku Ultima IV diffractometer over an angle range 2θ = 3-50° with scanning speed of 5° per minute. From powder diffractograms it is confirmed that **1**, **2**, **3** and **8** are isomorphic in nature as shown in Figure 31. PXRD pattern of **2** synthesized at room temperature (25 ^{o}C) and hydrothermal (120 °C) are same showing the formation of same products (see Figure 32).

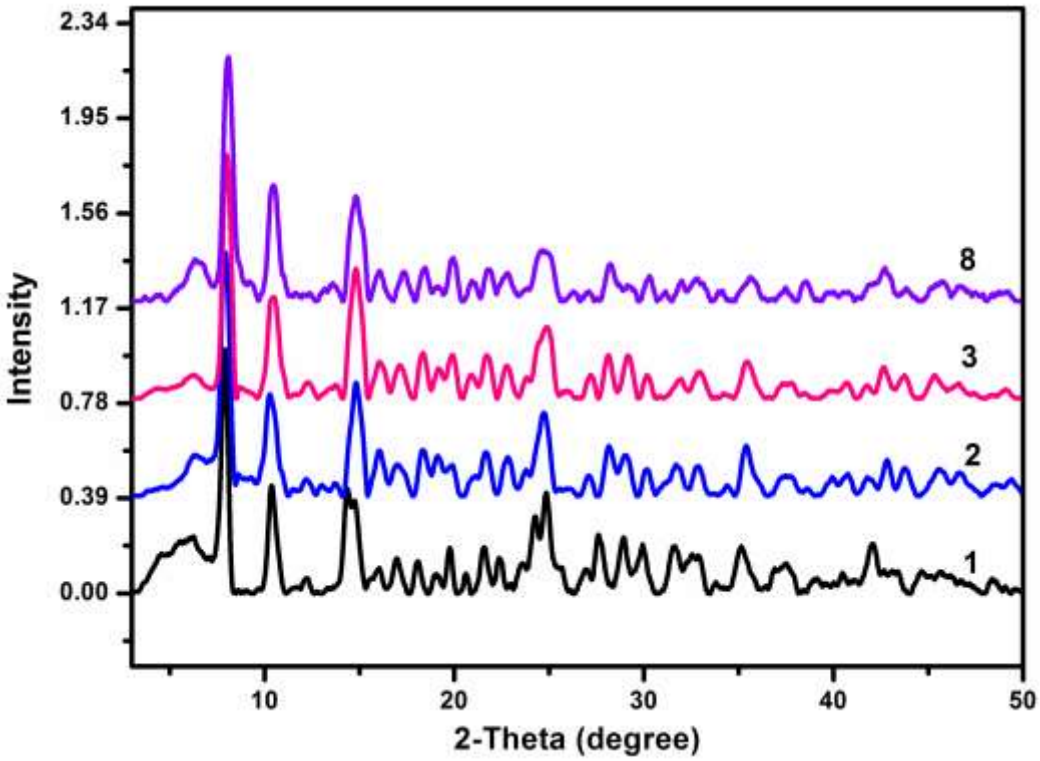

Figure 31. PXRD diffractogram of **1**, **2**, **3** and **8**.

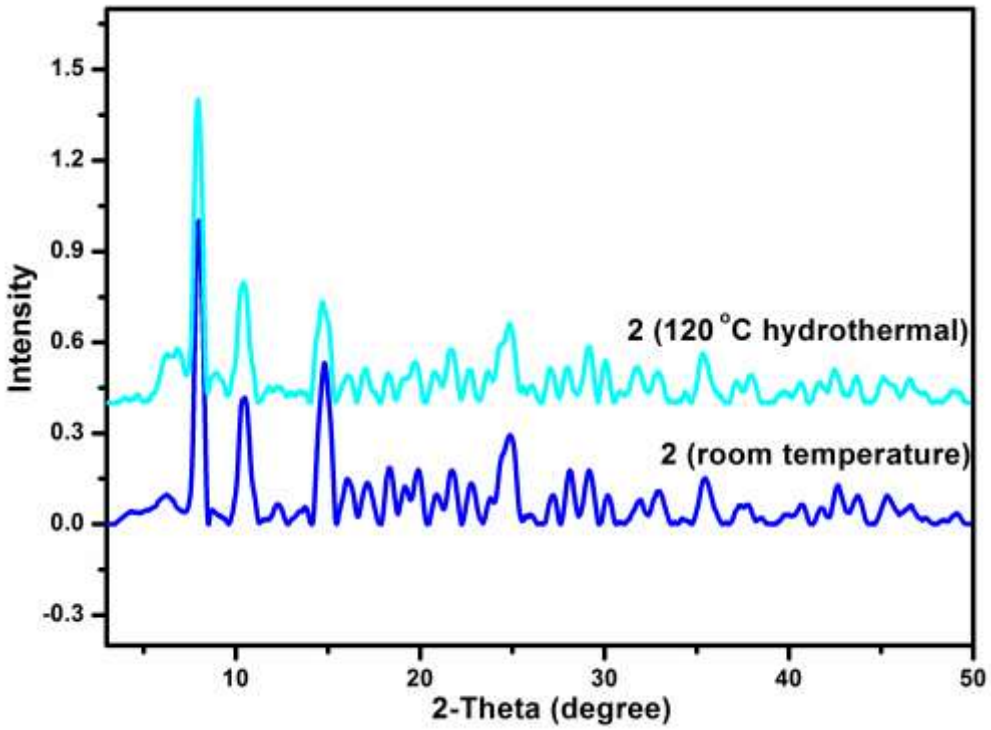

Figure 32. PXRD diffractograms of Complex **2** synthesized at hydrothermal and RT.

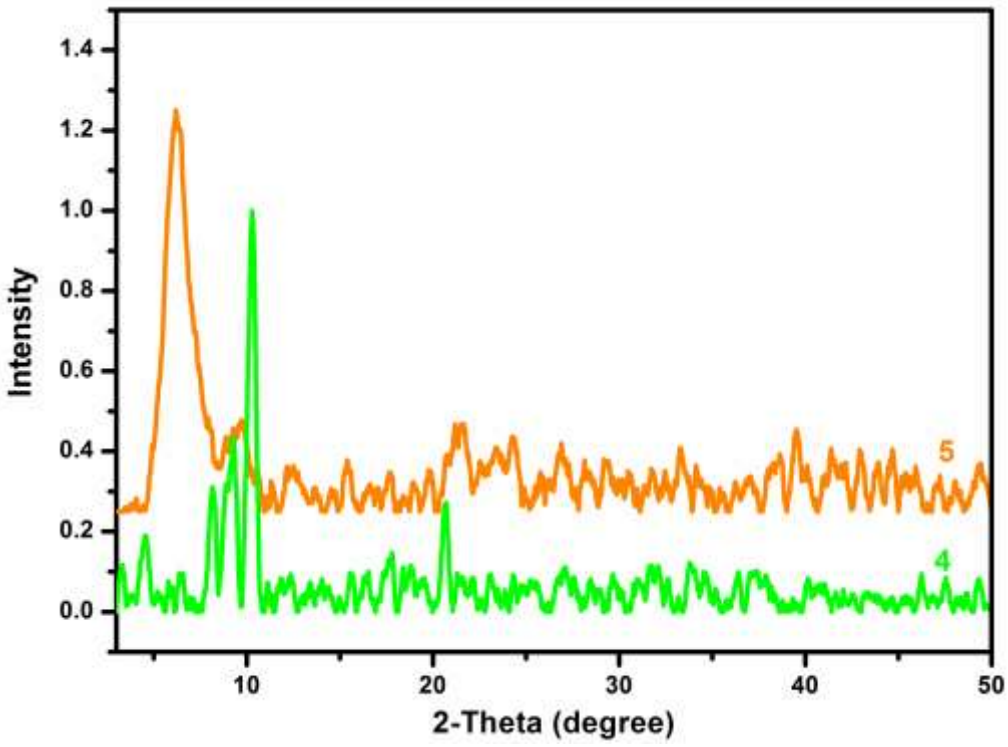

Figure 33. PXRD diffractogram of Complex **4** and **5**.

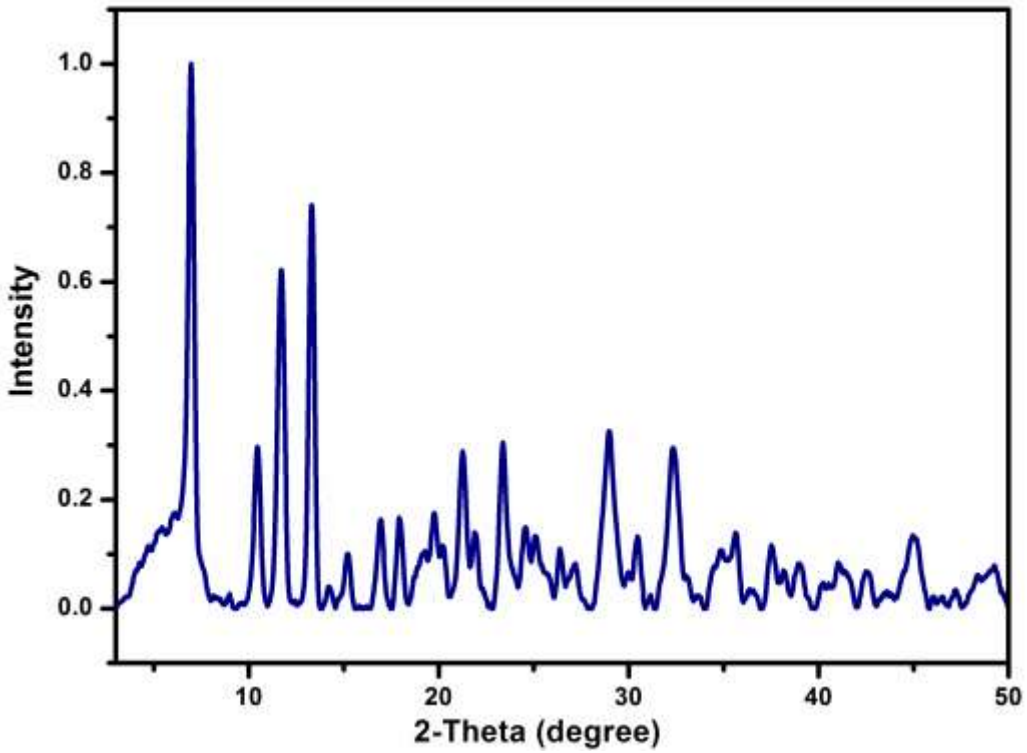

Figure 34. PXRD diffractogram of Complex **6**.

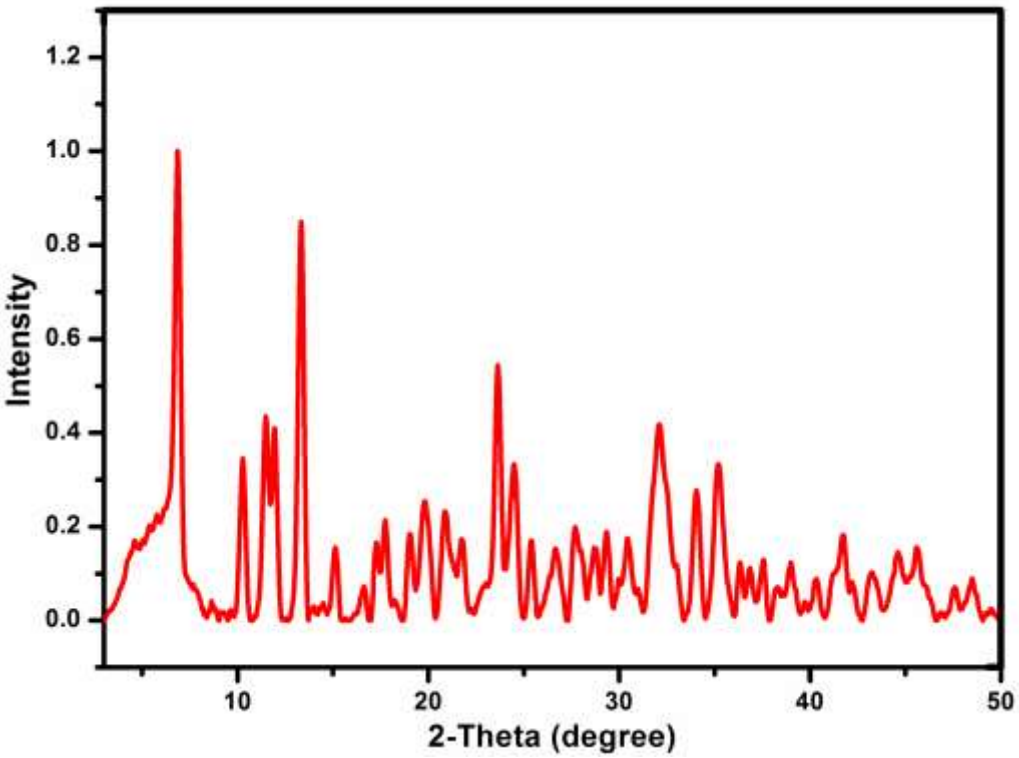

Figure 35. PXRD diffractogram of Complex **7**.

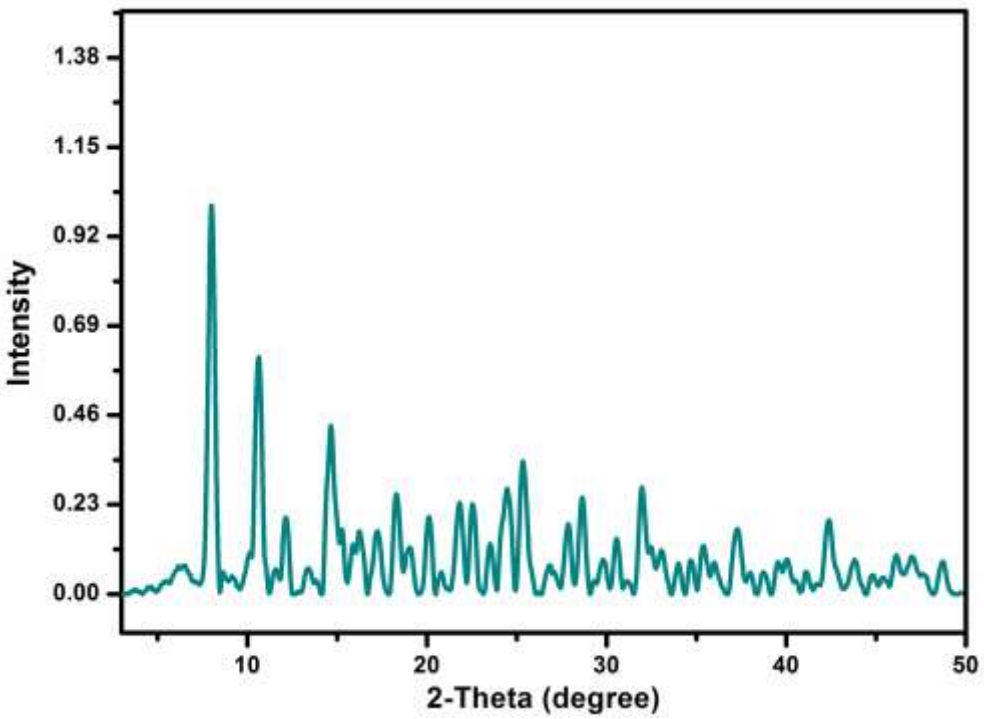

Figure 36. PXRD diffractogram of Complex **9**.

Field Emission Scanning Electron Microscopy (FESEM)

Surface morphology of these compounds were determined using FESEM (see Figures 37-41). Compounds **1**, **6** and **7** showed rod shaped morphology. Compounds **2** and **9** showed oval shaped morphology with microflowers (see Figures 37 and 41), compound **3** showed flakes type and compound **4** showed polyhedral type of morphology (see Figure 38), and compound **8** showed bar shaped surface morphology (see Figure 40).

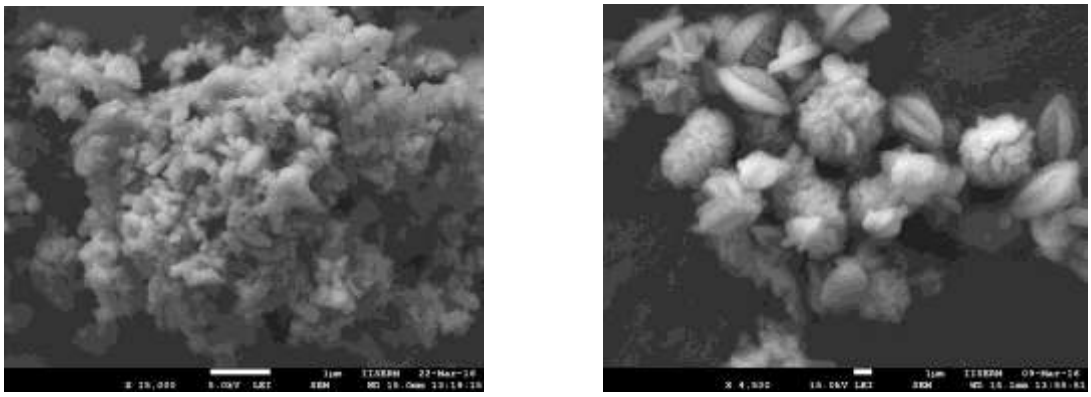

Figure 37. SEM micrograph of **1** (left) and (right) **2**.

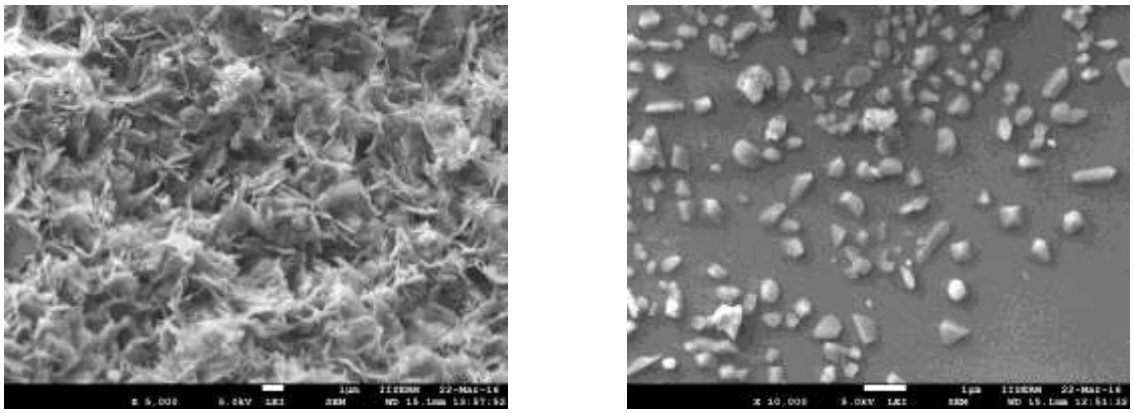

Figure 38. SEM micrograph of **3** (left) and **4** (right).

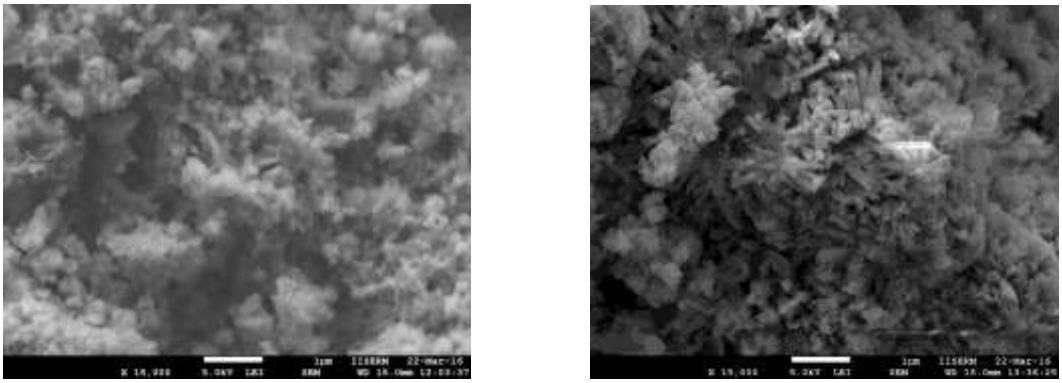

Figure 39. SEM micrograph of **5** (left) and **6** (right).

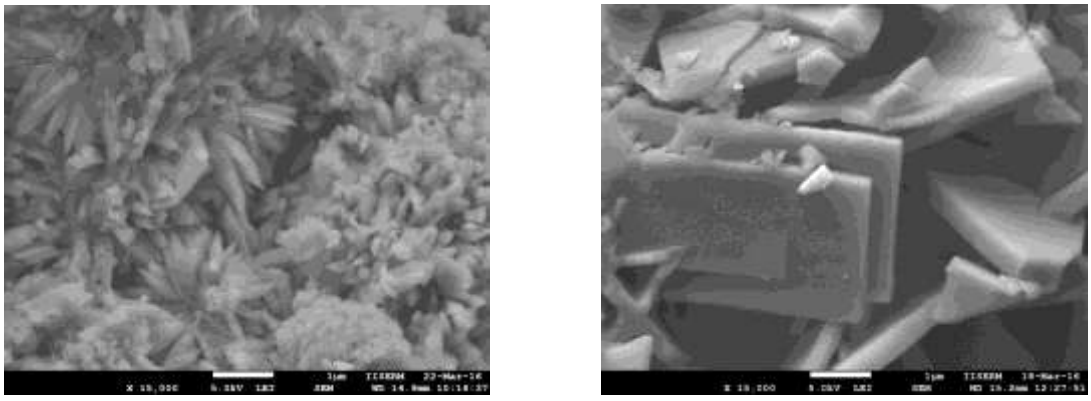

Figure 40. SEM micrograph of **7** (left) and **8** (right).

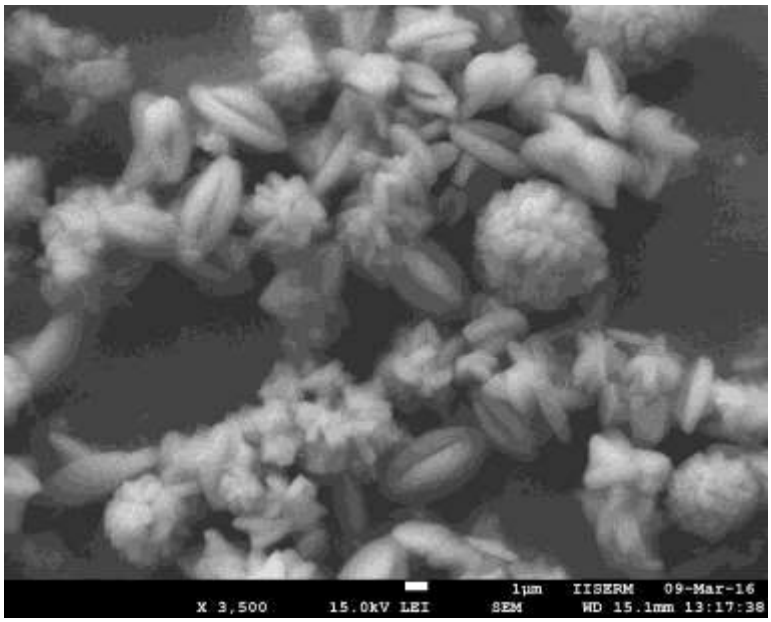

Figure 41. SEM micrograph of **9**.

Fluorescence Spectroscopy

The emission spectra of all complexes performed at room temperature as slurry, with concentration 2mg in 2mL DMSO, are displayed in Figures 42-47. The characteristic luminescent behaviours of these synthesized lanthanide MOFs suggest that the intramolecular energy transfers from the ligand to Ln(III). In case of Tb(III), intramolecular energy transfer is much more effective than those to Nd(III), Dy(III) and Sm(III) complexes.

[Nd(bpbd)(H$_2$O)$_2$NO$_3$]·7H$_2$O (2). The emission spectrum was measured in the 1100-1500 nm range with excitation wavelength 850 nm (see Figure 42). Luminescence spectra consist of three sharp and narrow characteristic optic bands centered at 1139, 1281, 1421 nm, which are attributed to the *f-f* transitions of $^4F_{3/2}$ (emitting level) $\rightarrow$ $^4I_{J/2}$ (J = 9, 11, 13).[54] The width of the three peaks are 25, 27 and 27 nm, respectively. The relative intensity sequence of these three transitions is $^4F_{3/2} \rightarrow {}^4I_{11/2} > {}^4F_{3/2} \rightarrow {}^4I_{9/2} > {}^4F_{3/2} \rightarrow {}^4I_{13/2}$.

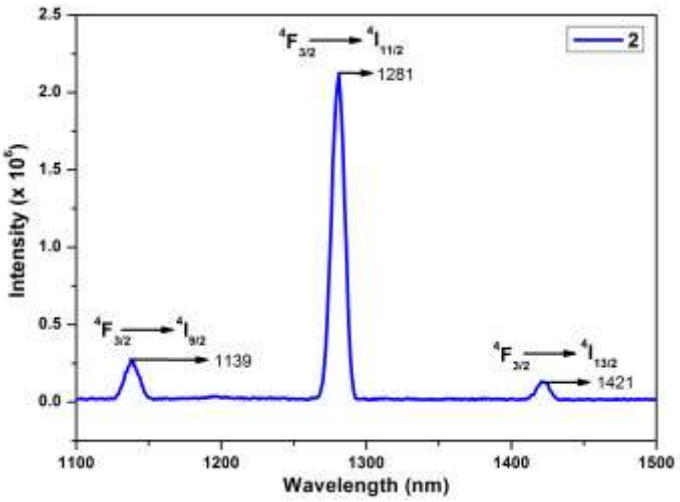

Figure 42. Emission spectrum of {[Nd(bpbd)(H_2O)$_2$$NO_3$]·7$H_2O$}$_n$ (**2**).

[Sm(bpbd)(H_2O)$_2$$NO_3$]·7$H_2O$ (**3**). The emission spectrum of **3** recorded at room temperature is shown in Figure 43. The emission spectrum was recorded by excitation the sample at 260 nm. The emission spectrum was measured from 555 to750 nm. Luminescence spectra consists of four characteristic optic bands centered at 564, 604, 648 and 707 nm, which are attributed to the *f-f* transitions of $^4G_{5/2}$ (emitting level) $\rightarrow$ $^6H_{J/2}$ (J = 5, 7, 9, and 11).[57] The emission band corresponding to 604 nm is the most intense which is for orange luminescence.

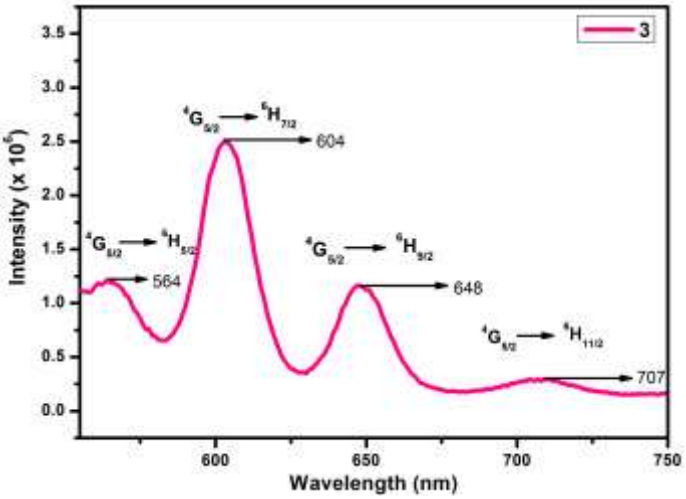

Figure 43. Emission spectrum of {[Sm(bpbd)(H_2O)$_2$$NO_3$]·7$H_2O$}$_n$ (**3**).

[Tb(bpbd)(H_2O)$_2$(NO_3)]·5H_2O (**4**)**.** It was excited at 340 nm and emission spectrum was collected in the range 470-650 nm and it displays a characteristic emission bands at 491, 547,

588, 623 nm and typical emission spectrum dominated by the hypersensitive $^5D_4 \rightarrow {}^7F_5$ transition.[54] The emission band corresponding to 547 nm is the most intense which corresponds to green luminescence as shown in Figure 44.

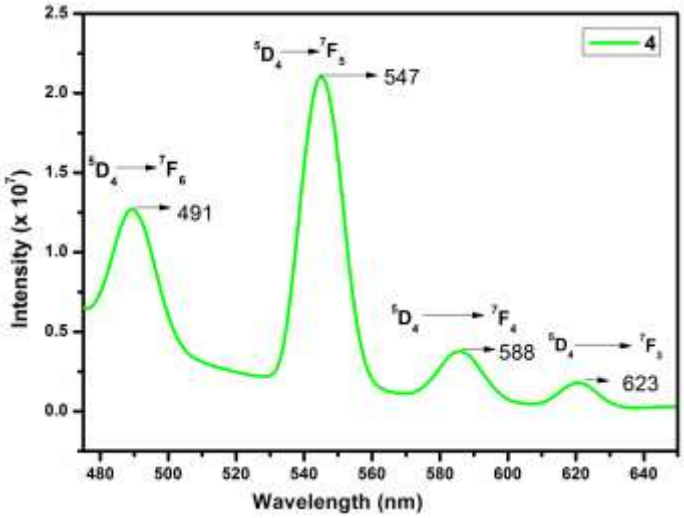

Figure 44. Emission spectrum of $\{Tb(bpbd)(H_2O)_2(NO_3)]\cdot 5H_2O\}_n$ (**4**).

$[Dy(bpbd)(H_2O)_2(NO_3)]\cdot 5H_2O$ (**5**). The photo-luminescence spectrum for complex **5** was recorded at room temperature. The excitation at 270 nm may result in second order interference thus to avoid that the emission spectra were recorded in two instant. The observed metal centered emission bands at 484 and 576 nm which corresponds to yellow luminescence, results from $^4F_{9/2} \rightarrow {}^6H_{15/2}$ and $^4F_{9/2} \rightarrow {}^6H_{13/2}$ transitions, respectively as shown in Figure 45.[57] A very weak signal at 664 nm which is attributed to $^4F_{9/2} \rightarrow {}^6H_{11/2}$ transition.[57]

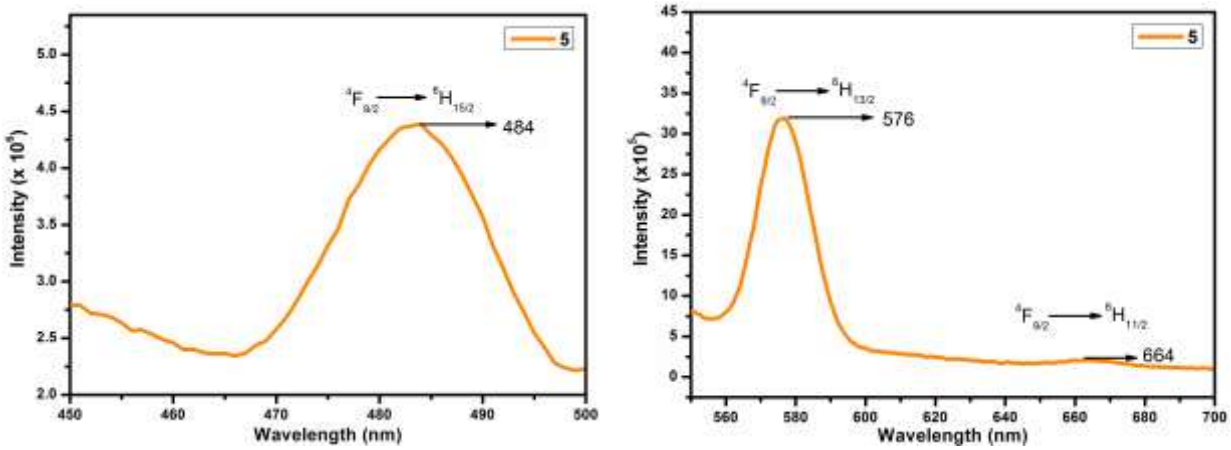

Figure 45. Emission spectrum of $\{Dy(bpbd)(H_2O)_2(NO_3)]\cdot 5H_2O\}_n$ (**5**).

[Nd(bpbd)(H$_2$O)$_2$(OAc)]·7H$_2$O (8). The emission spectrum was measured in the 900-1500 nm range with excitation wavelength 850 nm (see Figure 46). It consists of three characteristic optic bands centered at 1139, 1281 and 1421 nm, which are attributed to the *f-f* transitions of $^4F_{3/2}$ (emiting level) → $^4I_{J/2}$ (J = 9, 11 and 13).[54] The relative intensities of the $^4I_{9/2\text{-}13/2}$ bands are 1, 4.9, and 0.6, respectively.

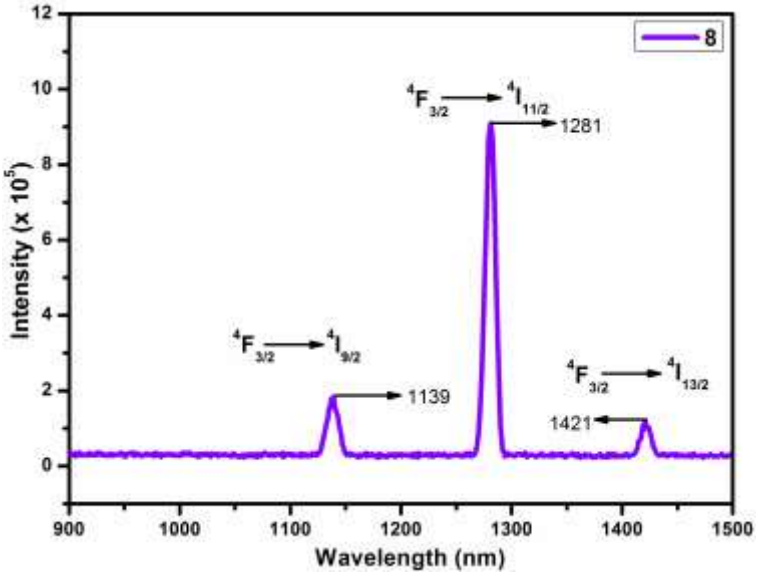

Figure 46. Emission spectrum of {[Nd(bpbd)(H$_2$O)$_2$(OAc)]·7H$_2$O}$_n$ (**8**).

[Nd(bpbd)(H$_2$O)$_2$(ClO$_4$)]·5H$_2$O (9). The emission spectrum was measured in the 900-1500 nm range with excitation wavelength 850 nm (see Figure 51). It consists of three characteristic optic bands centered at 1142, 1282 and 1422 nm, which are attributed to the *f-f* transitions of $^4F_{3/2}$ (emiting level) → $^4I_{J/2}$ (J = 9, 11 and 13).[54] The relative intensities of the $^4I_{9/2\text{-}13/2}$ bands are 1, 8.2, and 0.8 respectively.

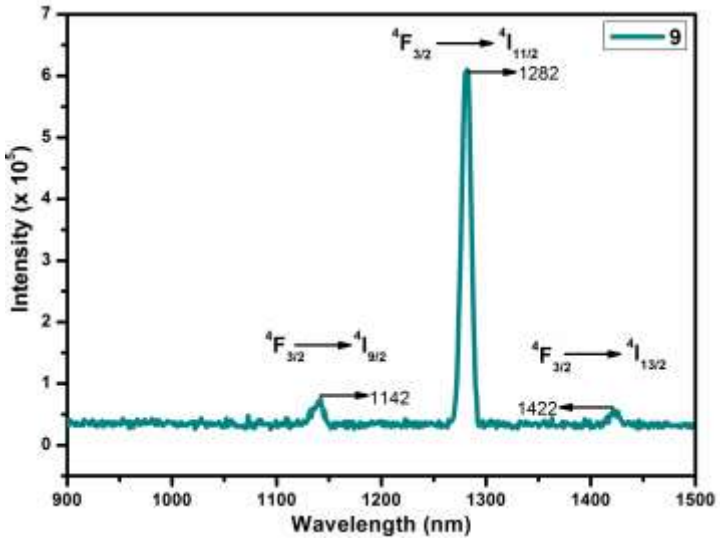

Figure 47. Emission spectrum of $\{[Nd(bpbd)(H_2O)_2(ClO_4)]\cdot 5H_2O\}_n$ **(9)**.

Sensing of Nitroaromatic Compounds

The detection of Picric acid (PA) is very crucial for environment safety. Picric acid is one of the violent explosive nitroaromatics, used in military operations; during its production and use it is released into environment which pollutes air, underwater, soil and bio-system.[58] Therefore, detection of nitro-aromatic compounds (NAC) has attracted the more attention from last decade. Here, highly luminescent MOFs of Nd(III) and Tb(III) are used to demonstrate as a selective sensor for the detection of nitroaromatic explosives via fluorescence quenching. Sensing based on fluorescence is gaining more attention because of its simplicity, selectivity and sensitivity. The nitroaromatic compounds (nitrobenzene (NB), dinitrobenzene (DNB), dinitrotoluene (DNT), trinitrotoluene (TNT) and trinitrophenol (PA)) are strong oxidizing agent, due to the presence of electron withdrawing group, and used as common commercial explosives. For selective sensing of picric acid using complexes **2**, **4**, **8** and **9**; picric acid (PA), nitrobenzene, dinitrobenzene and dinitrotoluene explosives were used.

*Nitroaromatics sensing by **4** (in DMSO)*

Complex **4** showed emission bands at 491, 547, 588 and 623 nm upon excitation at 340 nm (shown in Figure 44). On the basis of fluorescence property of the complex **4**, fluorescence sensing was carried out for various nitroaromatics in DMSO. The quenching efficiency % of the electron deficient nitroaromatics is plotted in Figure 48. The luminescence intensity at 547 nm is

monitored which decreases with gradual addition of 10 μL of nitroaromatics (0.002 M in DMSO), but decrease significantly when same amount of picric acid is added. According to the Stern-Volmer plots (see Figure 49), the quenching efficiency for the nitroaromatics in water was found to be the following order: TNP >> NB > DNB > 2, 4-DNT > 2, 6-DNT in case of **4**.

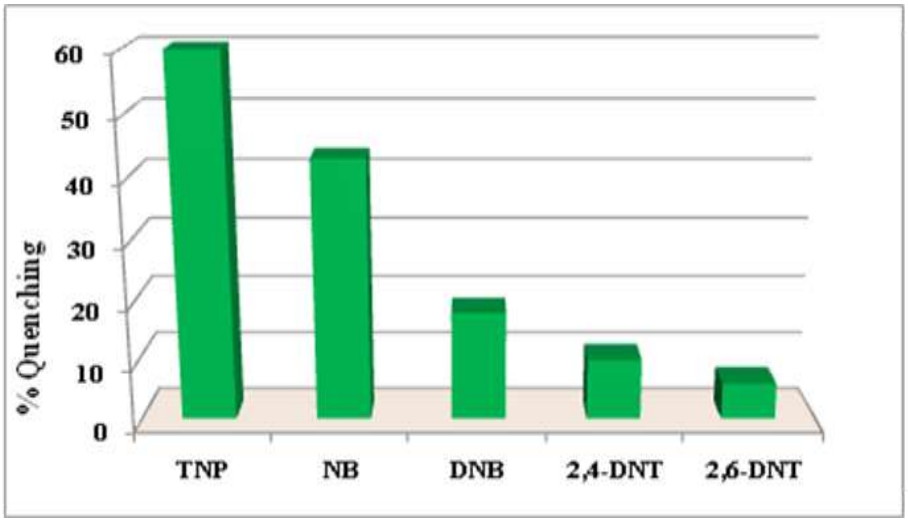

Figure 48. Percentage of fluorescence quenching of $^{5}D_{4} \rightarrow {}^{7}F_{5}$ (547 nm) observed for introducing different nitroaromatic compounds into the DMSO solution of **4**.

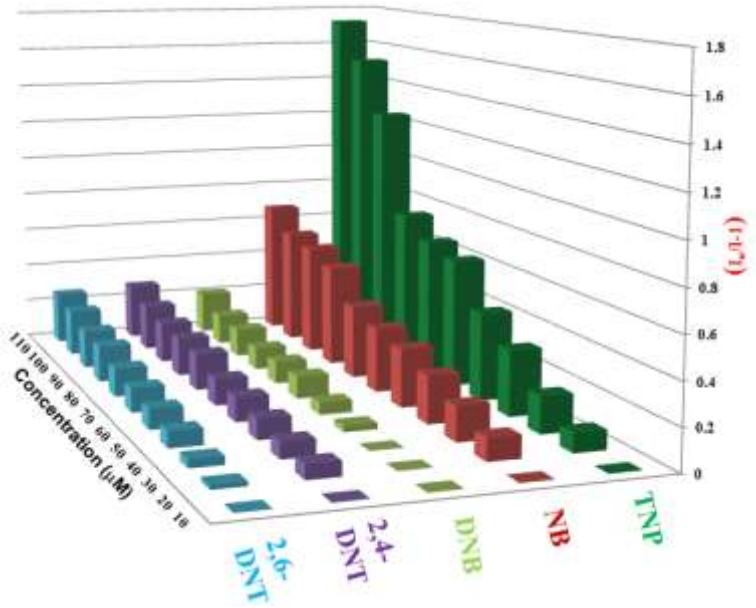

Figure 49. Comparison of quenching of **4** in DMSO by various analytes.

The fluorescence quenching efficiency by PA increased to 75% when the concentration of PA exceeded to 120 μL (see Figure 50). The calculated limit of detection for PA is 1 ppm based on 3σ/m value. This result indicates that complex **4** can selectively detect picric acid over other nitroaromatics, which is due to energy transfer, electron transfer and supramolecular interaction between PA and bpbd-Tb cluster. PA is described as 2,4,6-trinitrophenol, due to the presence of three electron withdrawing nitro group on the benzene ring, the hydroxyl group become more acidic and the ring become electron deficient. Therefore, the acidic hydrogen from PA can bind with oxygen of nitrate anion and form supramolecular interaction through hydrogen bonding. Other explanation can be electron transfer from electron rich picolinate moiety of bpbd-Tb cluster to electron deficient PA.

The fluorescence quenching efficiency was also investigated based on Stern-Volmer equation:[59]

$$\frac{I_o}{I} = K_{sv}[M] + 1$$

Where I is the intensity of analyte at concentration [M], I_o is the intensity before the addition of analyte, [M]=0 and K_{sv} is the quenching coefficient. Based on the plot, found Stern-Volmer constant for **4** is 2.1x 10^4 M^{-1} (Figure 51).

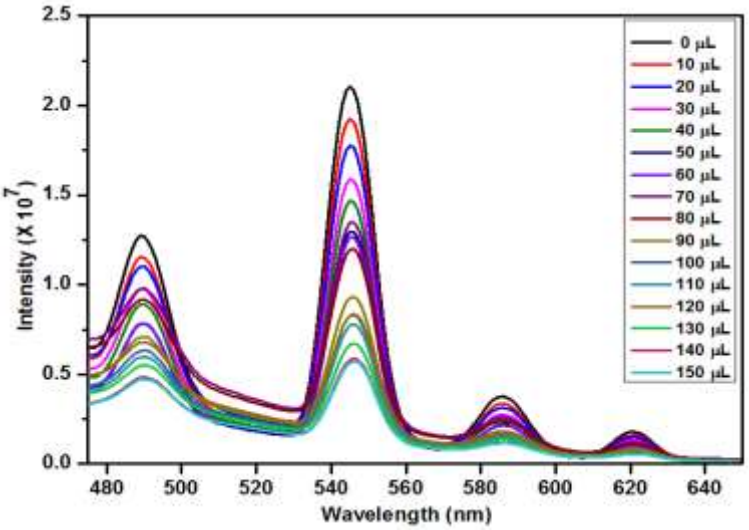

Figure 50. Fluorescence titration profile of **4** in DMSO by gradual addition of 10 μL of 0.002 M solution of picric acid in DMSO.

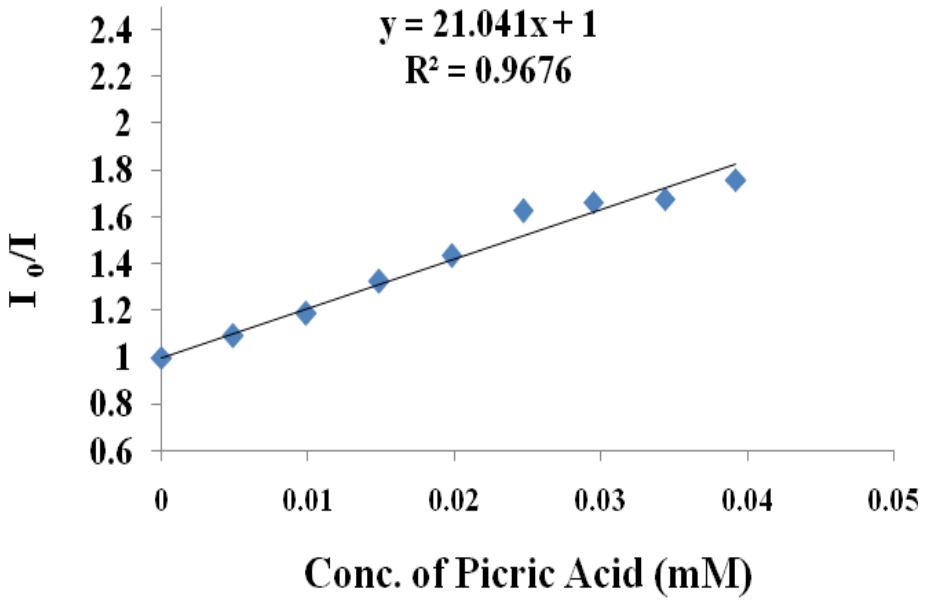

Figure 51. Stern-Volmer plot of complex **4**.

*Nitroaromatics sensing by **2**, **8** and **9** (in water)*

For Neodymium complexes, the emission bands are observed at 1139, 1281 and 1421 nm upon excitation at 850 nm (as shown in Figures 42, 46 and 47). Similar strategy is applied here as previous one. Fluorescence titration is done with monitoring at 1281 nm which decrease with gradual addition of 10 μL of nitroaromatics (0.002 M in water) added, but decrease significantly when same amount of picric acid is added in case of **2**, **8** and **9** (see Figures 52, 54 and 56, respectively). The detection limit for complex **2**, **8**, and **9** are 28, 9 and 3 ppm, respectively. The Stern-Volmer constants 1.2 x 10^5, 1.32 x 10^5 and 8.1 x 10^4 M^{-1} for **2**, **8** and **9**, respectively (see Figure 53, 55 and 57).

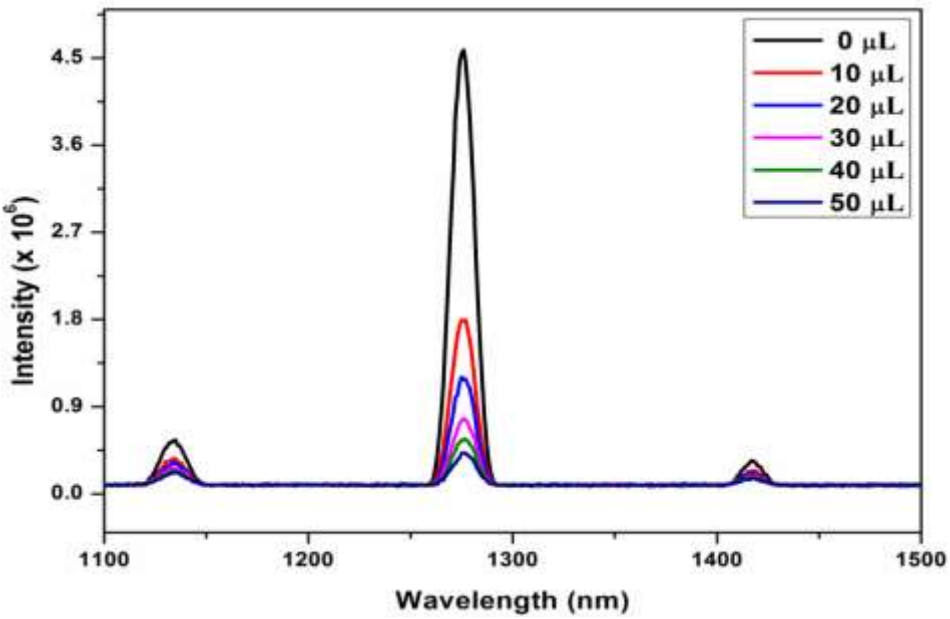

Figure 52. Fluorescence titration profile of **2** in water by gradual addition of 10 µL of 0.002 M solution of picric acid in water.

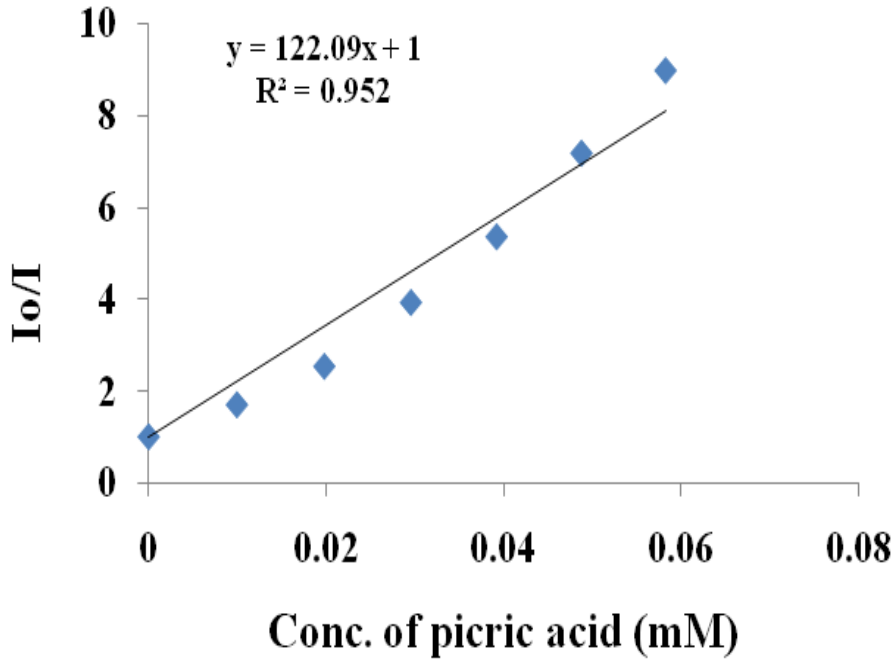

Figure 53. Stern-Volmer Plot of **2**.

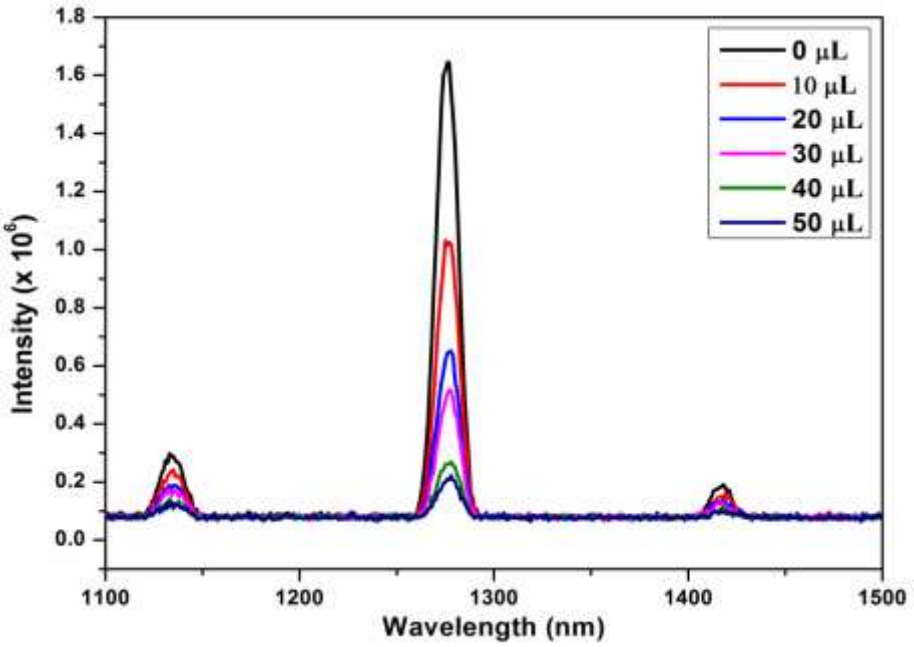

Figure 54. Fluorescence titration profile of **8** in water by gradual addition of 10 µL of 0.002 M solution of picric acid in water.

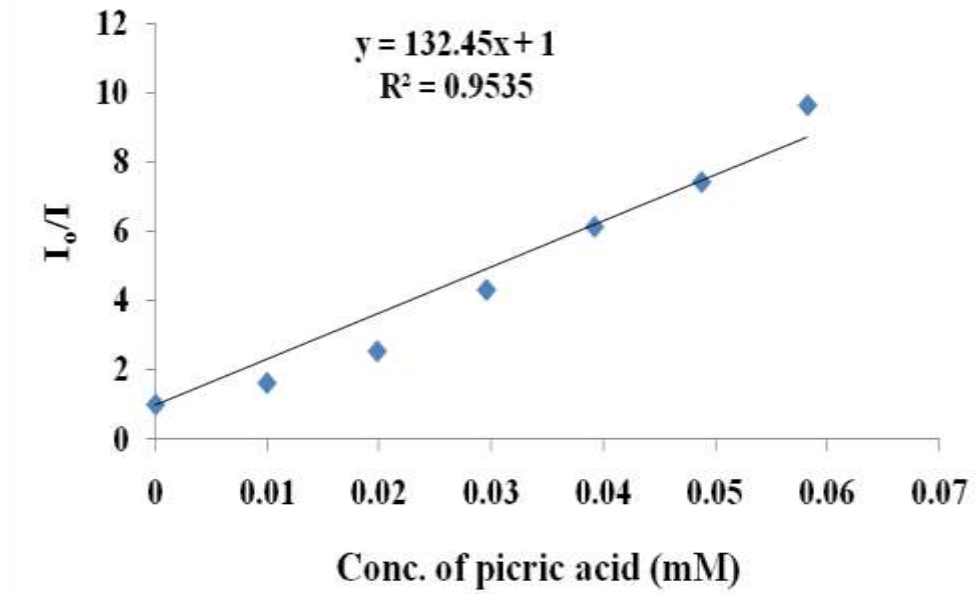

Figure 55. Stern-Volmer Plot of **8**.

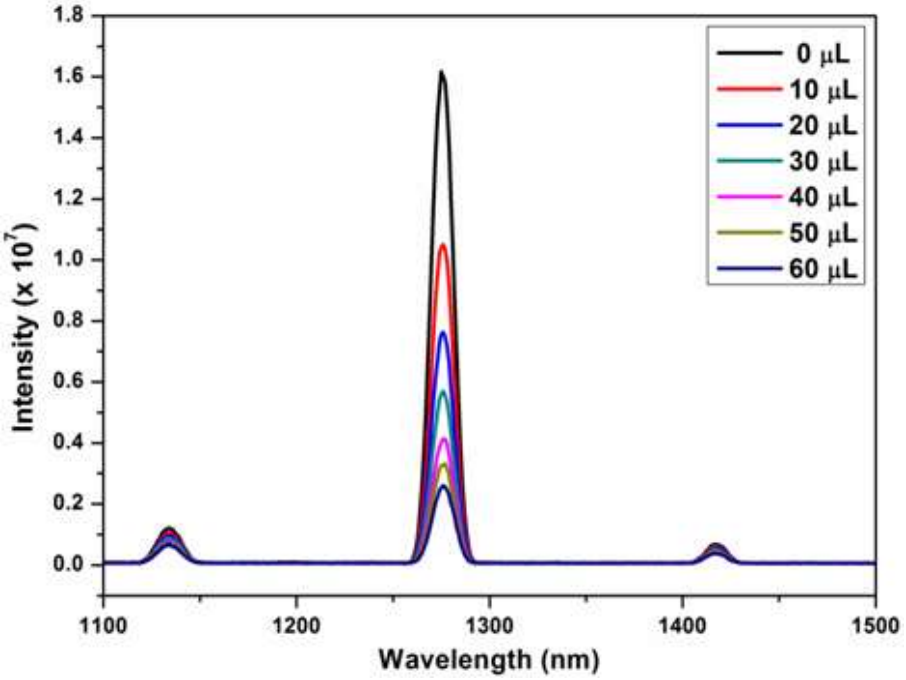

Figure 56. Fluorescence titration profile of **9** in water by gradual addition of 10 µL of 0.002 M solution of picric acid in water.

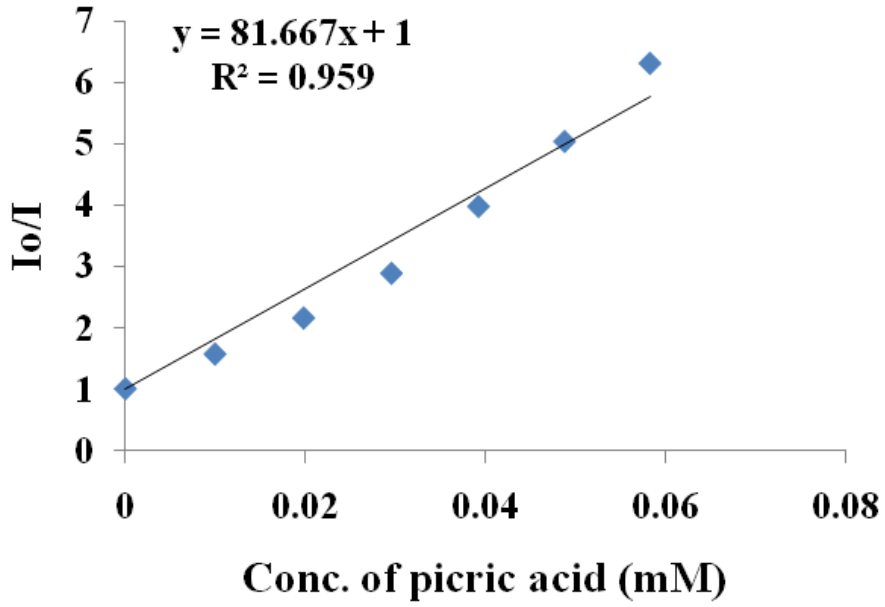

Figure 57. Stern-Volmer Plot of **9**.

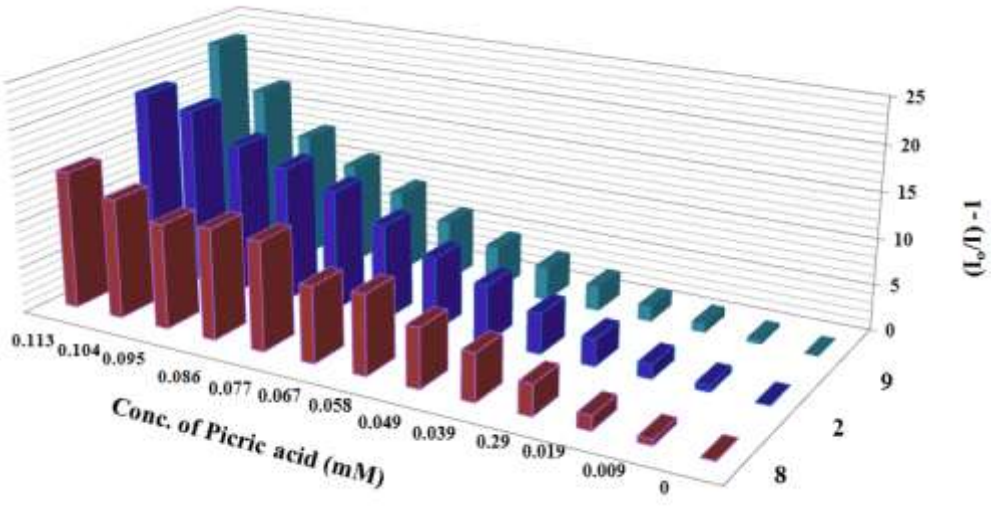

Figure 58. Comparison of PA sensing via complex **2**, **8** and **9**.

The high selectivity of picric acid sensing for complex **9** (see Figure 56) can be explained on the base of supramolecular interaction (*e.g.* hydrogen bonding) between anion and PA; because based on FTIR studies, perchlorate is in free form so it can form four hydrogen bond with per PA. The significant sensing of **9** on PA molecule in water at room temperature motivated to investigate its capabilities for the detection of the other nitroaromatics. The quenching efficiency % of the electron deficient nitroaromatics is plotted in Figure 59.

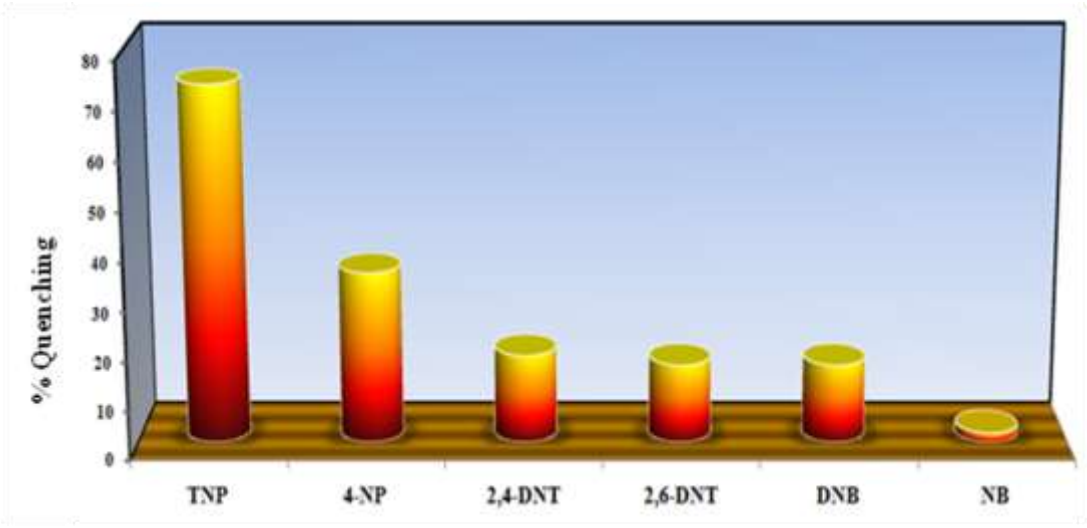

Figure 59. Percentage of fluorescence quenching of $^{4}F_{3/2} \rightarrow {}^{6}I_{11/2}$ (1281 nm) observed for introducing different nitroaromatic compound into the water suspension of **9**.

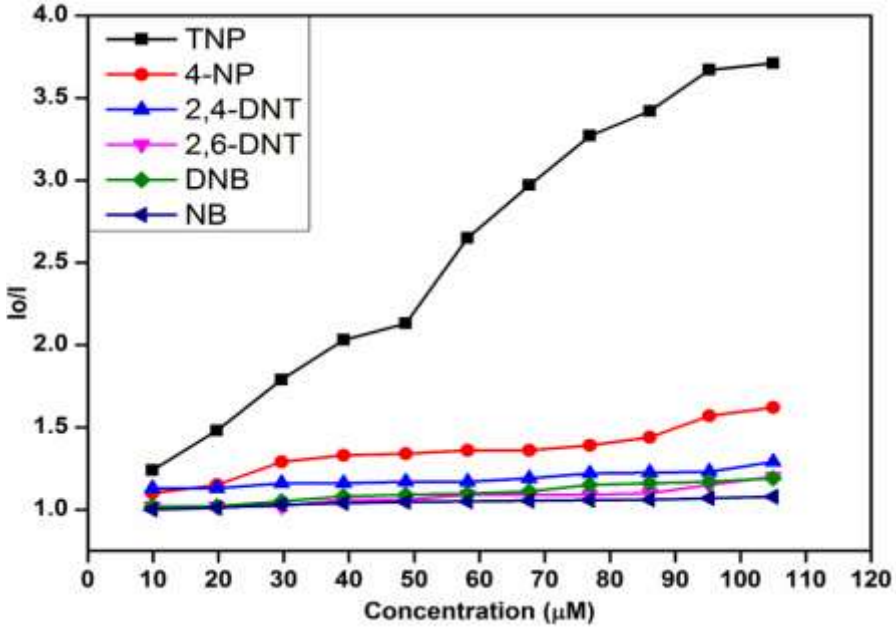

Figure 60. Comparison of K_{sv} curves with different nitroaromatics in case of **9**.

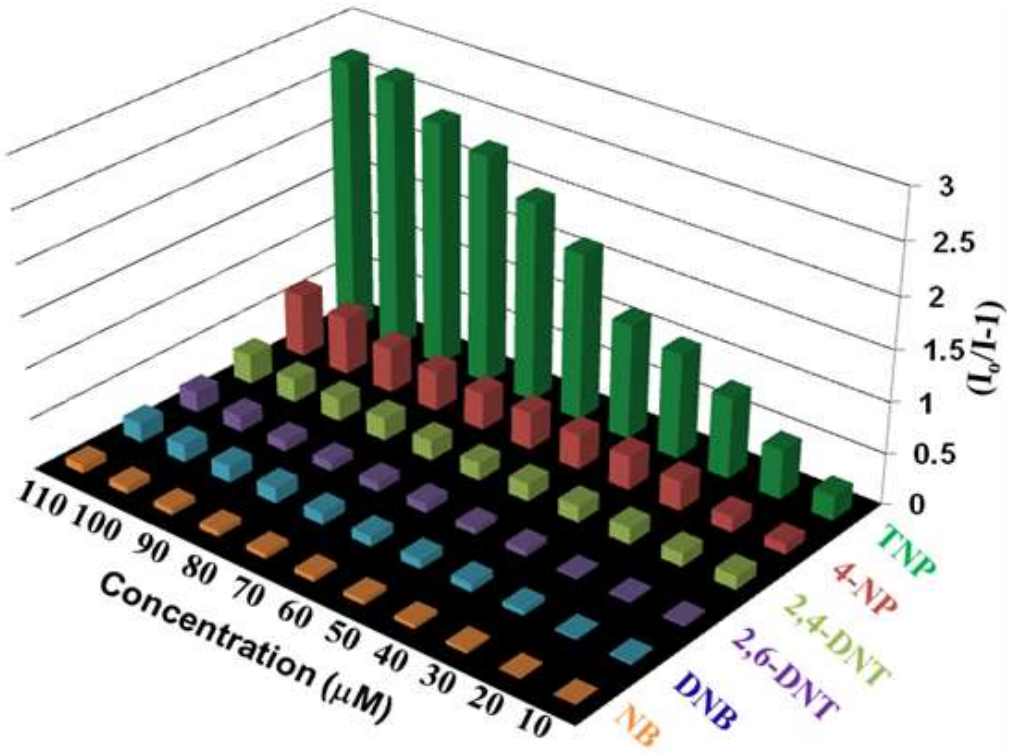

Figure 61. Comparison of Stern-Volmer plots of various analytes by **9** in water.

According to the Stern-Volmer plots (see Figure 61), the quenching efficiency for the nitroaromatics in water was found to be the following order: PA >> 4-NP > 2, 4-DNT > 2, 6-DNT ~ DNB > NB in case of **9**.

In order to understand the interaction of picric acid with **2** or **4**, a stoichiometric titration of an aqueous solution of picric acid by **2** or **4** was followed by UV-vis spectroscopy. As can be seen in Figures 62 and 63, a decrease in the peak intensity at 355 nm (due to picric acid) by the addition of **2** or **4** is observed while the peak due **2** or **4** at 262 nm is shifted to 252 nm. This indicates that there is a strong interaction between **2** or **4** and picric acid (PA) causing a change in the energy level at the metal center.

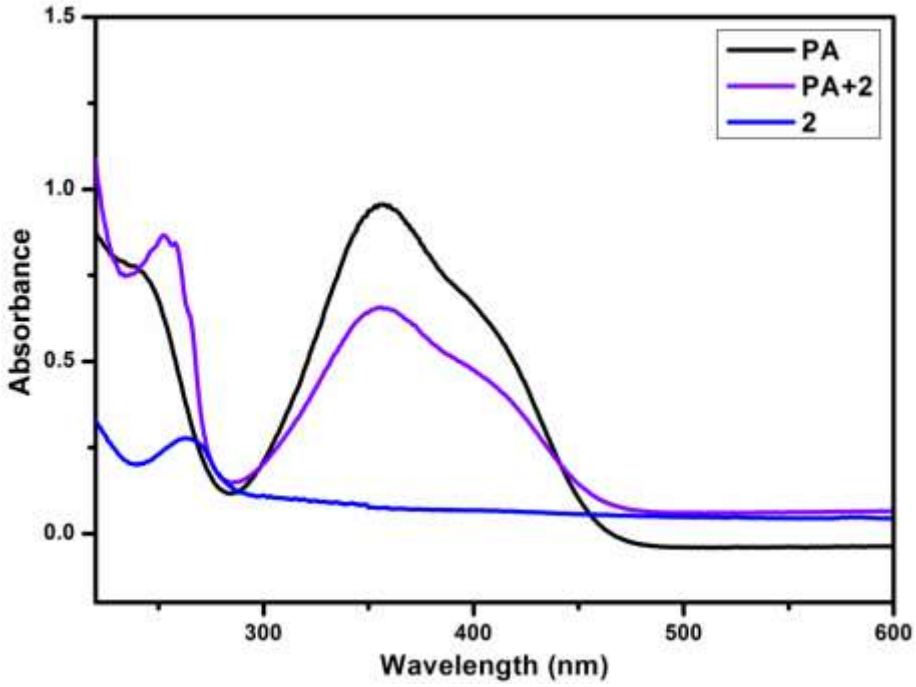

Figure 62. Change in abs. spectra of **PA** (black) in water upon addition of **2** (blue).

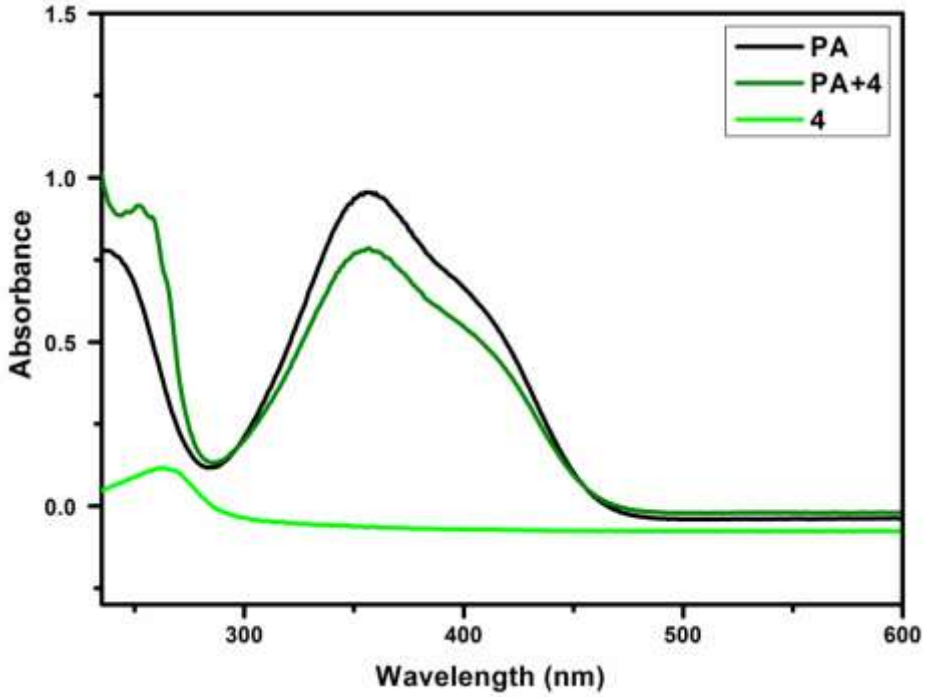

Figure 63. Change in abs. spectra of **PA** (black) upon addition of **4** (green).

Chapter IV

Conclusions and Future Directions

A systematic and careful designing of several lanthanide complexes followed by their structural characterization and photo-physical studies has provided a good starting point for this project. Using a new pyridine-carboxylate ligand, nine Lanthanide (La, Nd, Sm, Tb and Dy) complexes have been synthesised in good yields. All these complexes are well characterised by various analytical techniques, such as elemental analysis, UV-visible spectroscopy, FTIR spectroscopy, SEM/EDX, PXRD, TGA and Fluorescence spectroscopy (where applicable). Based on the PXRD and TGA data, compounds **1**, **2**, **3** and **8** are found to be isomorphous. FTIR spectroscopic data conclusively show chelating bidentate binding mode of the carboxylate and monodentate binding mode of nitrate. These complexes with the bpbd ligand were found to be stable in the solid state up to 220 °C. Complex **2** was synthesized under room temperature and hydrothermal conditions and showed the same structural features based on spectroscopic and PXRD data. SEM images confirmed 3D microflower nature for complexes **2** and **9**, polyhedral type for complex **4** and sheet shaped for complex **8**. All lanthanide MOFs show their characteristic visible and NIR luminescence through intramolecular energy transfer from ligand to the lanthanide centre. This fulfils the requirement to sensitize the luminescence of lanthanide ions such as Nd(III), Sm(III), Tb(III) and Dy(III). Complexes **2**, **4**, **8** and **9** showed selective sensing of picric acid over other nitroaromatic explosives with the lowest detection limit of 1 ppm for complex **4**. These complexes are considered as suitable class of sensor materials for selective sensing of picric acid.

For the sensing applications, it is necessary to incorporate quantum efficiency and life time measurements in future studies. Furthermore, sensing of other neutral molecules, anions and cations could be carried with the compounds reported in this work. The exploration of the Ln(III) complexes for catalysis, and magnetism will be exciting for both academia, military and industry purposes.

References

1. Davis, M. E. *Nature* **2002**, *417*, 813.
2. Inagaki, S.; Fukushima, Y.; Kuroda, K. *J. Chem. Soc. Chem. Comm.* **1993**, 680-682.
3. Imhof, A.; Pine, D. J. *Nature* **1997**, *389*, 948.
4. Cundy, C. S.; Cox, P. A. *Chem. Rev.* **2003**, *103*, 663.
5. http://www.spring8.or.jp/en/news_publications/research_highlights/no_58/
6. Haldara, R. and Maji, T.K. *CrystEngComm*, **2013**, *15*, 9276-9295.
7. James, S. L. *Chem Soc Rev.* **2003**, *32*, 276.
8. Cook, T. R.; Zheng, Y.R; Stang, P. J. *Chem. Rev*. **2013**, *113*, 734.
9. Cui, Y.; Yue, Y.; Qian, G. and Chen, B. *Chem. Rev*. **2012**, *112*, 1126.
10. Horike, S.; Dinca, M.; Tamaki, K.; Long, J. R. *J. Am. Chem. Soc*., **2008**, *130*, 5854.
11. Sabbatini, N.; Guardigli, M.; Lehn, J. M. *Coord.*,*Chem. Rev*. **1993**, *123*, 201.
12. Lee, E. Y.; Jang, S.Y.;Suh, M. P. *J. Am. Chem. Soc.*, **2005**, *127*, 6374.
13. Xiao, J. D.; Qiu, L. G.; Ke, F.; Yuan, Y. P.; Xu, G. S.; Wanga, Y. M.; Jianga, X. *J. Mater. Chem. A*, **2013**, *1*, 8745.
14. Chen, B. L.; Yang, Y.; Zapata, F.; Lin, G. N.; Qian, G. D.; Lobkovsky, E. B. *Adv. Mater*., **2007**, *19*, 1693.
15. Chen, B.; Wang, L.; Zapata, F.; Qian, G.; Lobkovsky, E. B. *J. Am. Chem. Soc.* **2008**, *130*, 6718.
16. (a) Devic, T.; Serre, C.; Audebrand, N.; Marrot, J.; Ferey, G. *J. Am. Chem. Soc.* **2005**, *127*, 12788. (b) Chandler, B. D.; Yu, J. O.; Cramb, D. T.; Shimizu, G. K. H. *Chem. Mater.* **2007**, *19*, 4467.
17. Rosi, N. L.; Kim, J.; Eddaoudi, M.; Chen, B. L.; Keeffe, M.; Yaghi, O. M. *J. Am. Chem. Soc*. **2005**, *127*, 1504.
18. Luo, J.; Xu, H.; Liu, Y.; Zhao, Y.; Daemen, L. L.; Brown, C.; Timofeeva, T. V.; Ma, S.; Zhou, H.-C. *J. Am. Chem. Soc*. **2008**, *130*, 9626.
19. He, H.; Yuan, D.; Ma, H.; Sun, D.; Zhang, G.; Zhou, H. C. *Inorg. Chem*. **2010**, *49*, 7605.
20. Kaden, T. A. *Dalton Trans.*, **2006**, 3617.
21. Hemmila, I.; Mukkala, V. M. *Crit. Rev. Clin. Lab. Sci.*, **2001**, *38*, 441.
22. a) Laufer, R. B. *Chem. Rev*. **1987**, *87*, 901.b) Caravan, P.; Ellison, J. J.; McMurry, T. J.;

Laufer, R. B. *Chem. Rev*. **1999**, *99*, 2293.

23. (a) Wohnert, J.; Franz, K. J.; Nitz, M.; Imperiali, B.; Schwalbe, H. *J. Am. Chem. Soc.* **2003**, *125*, 13338.(b) Prudencio, M.; Rohovec, J.; Peters, J. A.; Tocheva, E.; Boulanger, M. J.; Murphy, M. E. P.; Hupkes, H. J.; Kosters, W.; Impagliazzo, A.; Ubbink, M. *Chem. Eur. J*. **2004**, *10*, 3252.
24. (a) Beeby, A.; Botchway, S. W.; Clarckson, I.; Faulkner, S.; Parker, A. W.; Parker D.; Williams, J. A. G. *J. Photochem. Photobiol., B*, **2000**, *57*, 83.(b) Charbonniere, L. J.; Hildebrandt, N.; Ziessel, R.; Lohmannsroben, H. G. *J. Am. Chem. Soc.*, **2006**, *128*, 12800.
25. Hildebrandt, N.; Charbonnire, L.; Lchmannsrcben, H.-G.; Ziessel, R. *Angew. Chem.* **2005**, *117*, 7784. (b) Faulkner, S.; Pope, S. J. A.; Burton-Pye, B.P. *Applied Spectroscopy Reviews*, **2005**, *40*, 1.
26. Shionoya, S.; Yen, W. M. Phosphor Handbook, CRC Press Inc., Boca Raton, Florida 33431, USA, **1999**.
27. Reyes, R.; Cremona, M.; Teotonio, E. E. S.; Brito, H. F, Malta, O. L. Chem. *Phys.Lett*., **2004**, *396*, 54.
28. Kido, J.; Okamoto, Y. *Chem. Rev*., **2002**, *102*, 2357.
29. Bunzli, J. C. G.; Comby, S.; Chauvin, A. S.; Vandevyver, C. D. B. *Journal of Rare Earths*, **2007**, *25*, 257.
30. Kuriki, K.; Koike, Y.; Okamoto, Y. *Chem. Rev*., **2002**, *102*, 2347.
31. https://harmoniaphilosophica.files.wordpress.com/2011/04/periodic_table_2012-06-01.jpg
32. Cotton, S., Lanthanide and Actinide Chemistry. John Wiley: Chichester, **2006**.
33. Chen, Y.; Ma, S. *Rev. Inorg. Chem*. **2012**, *32*, 81.
34. Atkins, P. W. "Quanta,2nd Ed.", **1991**, Oxford University Press.
35. Bruce, J. I.; Lowe, M. P.; Parker, D., *Photophysical Aspects of Lanthanide(III) Complexes. In The Chemistry of Constrast Agents in Medical Magnetic Resonance Imaging*, Merbach, A.E.; Toth, E., Eds. John Willey & Sons: **2001**; 437-460.
36. Comby, S.; Bunzli, J.C.G. Lanthanide Near-Infrared Luminescence in Molecular Probes and Devices In *Handbook on the Physics and Chemistry of Rare Earths*, Karl A. Gschneidner, J.J.- C.B.; Vitalij, K. P., Eds. Elsevier: Amsterdam, **2007**; Vol. 37, 217-470.

37. Bunzli, J. C.; Eliseeva, S.V. Basics of Lanthanide Photophysics. In *Lanthanide Spectroscopy, Materials and Bio-Applications*, Hanninen, P.; Harma, H., Eds. Springer: **2009**; Vol. 7.
38. Valeur, B.; Berberan-Santos, M. N. *J. Chem. Educ.* **2011**, *88*, 731.
39. Bunzli, J-C. G.; Piguet, C. *Chem. Soc. Rev.* **2005**, *34*, 1048.
40. Balzani, V.; Bergamini, G.; Campagna, S.; Puntoriero, F. *Top Curr Chem* **2007**, *280*, 1..
41. Bunzli, J. C. G., *Chemistry Letters* **2009**, *38*, 104.
42. Moore, E. G.; Samuel, A.P. S.; Raymond, K. N. *Acc. Chem. Res* **2009**, *42*, 542.
43. Bunzli, J.C.G.; Piguet, C. *Chem. Soc. Rev.*, **2005**, *34*, 1048.
44. Horrocks, W. D.; Sudnick, D. R. *J. Am. Chem. Soc.*, **1979**, *101*, 334.
45. Weissmann, S. I. *J. Chem. Phys.* **1942**, *10*, 214.
46. http://www.cchem.berkeley.edu/knrgrp/ln.html
47. (a) Bunzli, J. C. *Acc. Chem. Res.* **2006**, *39*, 53. (b) Pandya, S.; Yu, P. *Dalton Trans.* **2006**, 2757. (c) Gunnlaugsson, T.; Leonard, J. P. *Chem. Commun*. **2005**, 3114. (d) Faulkner, A.; Pope, S. J. A.; Burton-Pye, B. P. *Appl. Spec. Re*v. **2004**, *39*, 1. (e) Parker, D. *Chem. Soc. Re*v. **2004**, *33*, 156.
48. Hemmila, I.; Webb, S. *Drug Discovery Today* **1997**, *2*, 373.
49. Kropp, J. L.;Windsor, M.W. *J. Chem. Phys*., **1963**, *39*, 2769.
50. Kropp, J. L.;Windsor, M.W. *J. Chem. Phys*., **1965**, *42*, 1599.
51. Chauvin, A.-S.; Gumy, F.; Imbert, D.; Bunzli, J.C. *Spectrosc. Lett.* **2004**, *37*, 517.
52. Wu, J. Y.; Yeh, T. T.; Wen, Y. S.; Twu, J.; Lu, K. L. *Cryst. Growth Des.* **2006**, *6*, 467. (b) Grenthe, I. *J. Am. Chem. Soc.* **1961**, *83*, 360. (c) Horrocks, W. D.; Sundnick, D. R. *Science* **1979**, *206*, 1194. (d) Brayshaw, P. A.; Bunzli, J. C. G.; Froidevaux, P.; Harrowfield, J. M.; Kim, Y.; Sobolev, A. N. *Inorg. Chem.* **1995**, *34*, 2068.
53. Chatterton, N.; Bretonniere, Y.; Pecaut, J.; Mazzanti, M. *Angewandte Chemie-International Edition* **2005**, *44*, 7595.
54. Marchal, C.; Filinchuk, Y.; Chen, X. Y.; Imbert, D.; Mazzanti, M. *Chem. Eur. J*. **2009**, *15*, 5273.
55. Chatterton, N.; Gateau, C.; Mazzanti, M.; Pecaut, J.; Borel, A.; Helm, L.; Merbach, A. *Dalton trans*. **2005**,1129.
56. Caravan, P.; Mehrkhodavandi, P.; Orvig, C. *Inorg. Chem.* **1997**, *36*, 1316.

57. Gu, Z. G.; Fang, H. C.; Yin, P. Y.; Tong, L.; Ying, Y.; Hu, S. J.; Li, W. S.; Cai, Y. P. *Cryst. Growth Des*. **2011**, *11*, 2220.

58. Shanmugaraju, S.; Joshi, S. A.; Mukherjee, P. S. *J. Mater. Chem*. **2011**, *21*, 9130.

59. Rose, A.; Zhu, Z.; Madigan, C. F.; Swager, T. M.; Bulovic, V. *Nature* **2005**, *434*, 876.